

**MINERALOGICAL STUDY OF THE PLATINUM-  
GROUP ELEMENT DISTRIBUTION AND ASSOCIATED  
MINERALS FROM THREE STRATIGRAPHIC LAYERS,  
BIRD RIVER SILL, MANITOBA**

**L.J. CABRI and J.H.G. LAFLAMME**  
*Mineral Processing Laboratory*

*MINERAL SCIENCES LABORATORIES*  
**CANMET REPORT CM88-1E**

*April 1988*

© Minister of Supply and Services Canada 1989

Available in Canada through

Associated Bookstores  
and other booksellers

or by mail from

Canadian Government Publishing Centre  
Supply and Services Canada  
Ottawa, Canada K1A 0S9

Catalogue No. M38-13/88-1E

ISBN 0-660-13117-X

# MINERALOGICAL STUDY OF THE PLATINUM-GROUP ELEMENT DISTRIBUTION AND ASSOCIATED MINERALS FROM THREE STRATIGRAPHIC LAYERS, BIRD RIVER SILL, MANITOBA

by

L.J. Cabri\* and J.H.G. Laflamme\*\*

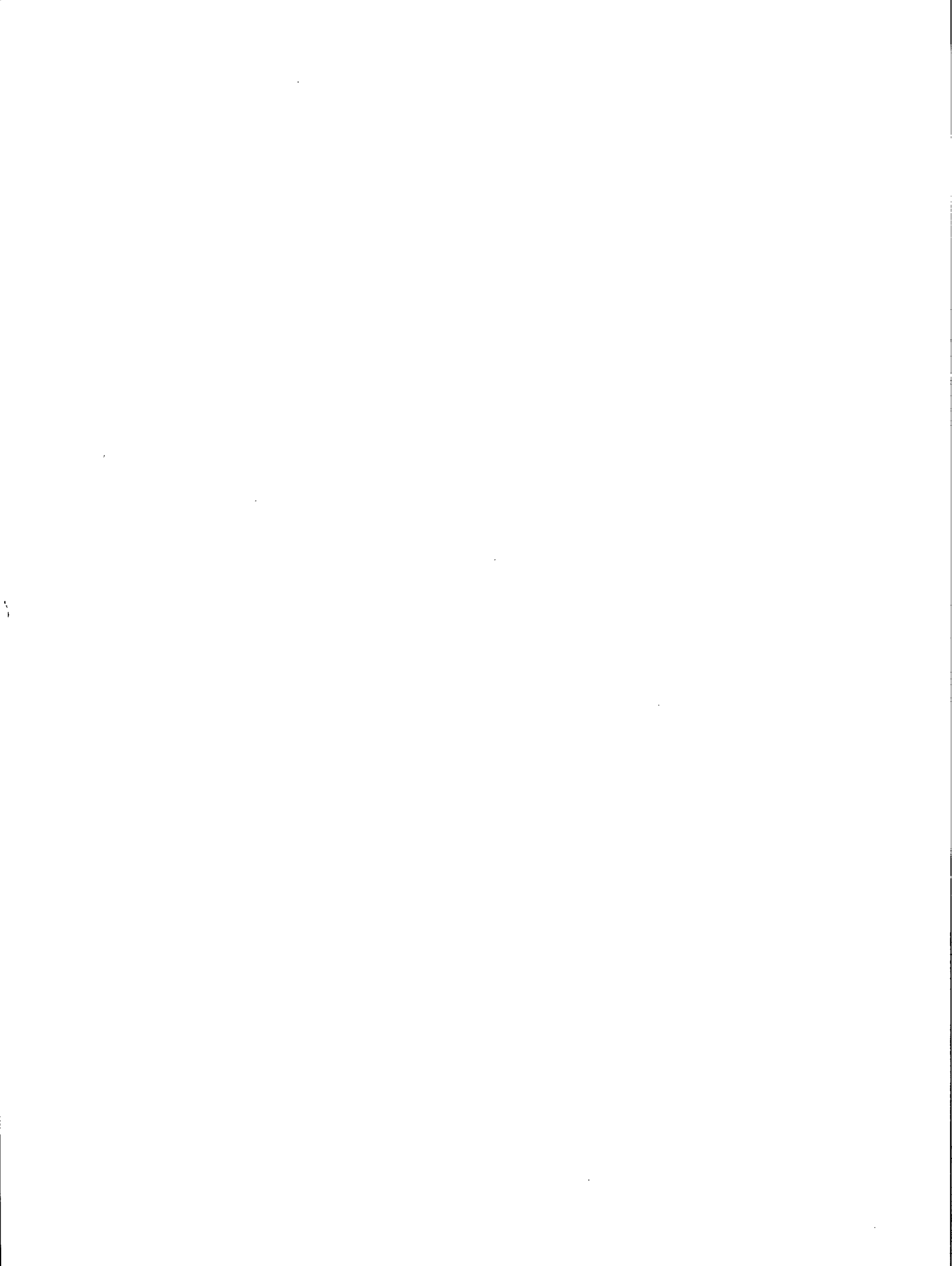
## Abstract

A preliminary mineralogical investigation of a total of nine hand samples from the Upper Main Chromitite, Lower Main Chromitite and the Lower Group platinum-bearing zone (Scoates et al., 1987) has shown a contrasting distribution of platinum-group elements. The Upper and Lower Main Chromitites contain laurite as the principal platinum-group mineral (PGM), followed by Os-Ir-Ru alloys, rare erlichmanite, irarsite and an unidentified PGM. Chromite is host to 43 vol % of the PGM; the balance occurs as inclusions in silicates (mainly clinocllore). In contrast, nine PGM occur in the Lower Group platinum-bearing zone, the most common of which are sperrylite and laurite. Kotulskite, merenskyite, hollingworthite, keithconnite and irarsite are less common, and mertieite II and another unidentified PGM are even more rare. Also, in contrast to the stratigraphically higher chromitites, 99 vol % of the PGM in the Lower Group platinum-bearing zone are included in silicates or sulphides, with the remaining 1 vol % in chromite and magnetite.

Chromite in the Upper and Lower Main Chromitites has 43-46% Cr<sub>2</sub>O<sub>3</sub> and contains irregular patches and rims of higher Cr<sub>2</sub>O<sub>3</sub> content (57-58%). The chromite is associated principally with clinocllore and grossular garnet. The texture of chromite in the Lower Group platinum-bearing zone is much more variable, and the Cr<sub>2</sub>O<sub>3</sub> content is lower (37-40%). Magnetite is predominant in some samples, whereas clinocllore and serpentine are common silicates. Proton microprobe analyses of chromite from all three sample types have indicated trace contents of Ni, Zn and Ga.

---

\*Research Scientist and \*\*Mineralogical Technician, Process Mineralogy Section, Mineral Processing Laboratory, Mineral Sciences Laboratories, CANMET, Energy, Mines and Resources Canada, Ottawa, Ontario K1A 0G1.



# ÉTUDE MINÉRALOGIQUE DE LA DISTRIBUTION DES ÉLÉMENTS DU GROUPE DU PLATINE ET DES MINÉRAUX ASSOCIÉS PROVENANT DE TROIS COUCHES STRATIGRAPHIQUES, BIRD RIVER SILL (MANITOBA)

par

L.J. Cabri\* et J.H.G. Laflamme\*\*

## Résumé

Un examen minéralogique préliminaire d'un ensemble de neuf échantillons prélevés à la main dans les chromitites principales supérieure et inférieure et dans la zone platinifère du groupe inférieur (Scoates et coll., 1987) a révélé une distribution contrastante des éléments du groupe du platine. Les chromitites principales supérieure et inférieure contiennent de la laurite comme principal minéral du groupe du platine (MGP), des alliages Os-Ir-Ru, très peu d'erlichmanite, de l'irarsite et un MGP non identifié. La chromite loge jusqu'à 43 % en volume des MGP : le reste se trouve sous forme d'inclusions dans des silicates (surtout du clinocllore). Par contre, on trouve neuf MGP dans la zone platinifère du groupe inférieur, les plus communs étant la sperrylite et la laurite. La kotulskite, la mérenskyite, la hollingworthite, la keithconnite et l'irarsite sont moins abondantes, et la mertiéite II et un autre MGP non identifié sont encore plus rares. Aussi, à l'opposé des chromitites qui sont stratigraphiquement plus élevées, 99 % en volume des MGP dans la zone platinifère du groupe inférieur sont logés dans des silicates ou des sulfures, l'autre 1 % en volume se trouvant dans de la chromite et de la magnétite.

La chromite dans les chromitites principales supérieure et inférieure contient 43-46 % de  $\text{Cr}_2\text{O}_3$  et, par endroits, des zones et des bordures plus riches en  $\text{Cr}_2\text{O}_3$  (57-58 %). La chromite est associée principalement à du clinocllore et du grenat grossulaire. La texture de la chromite dans la zone platinifère du groupe inférieur est beaucoup plus variable, et la teneur en  $\text{Cr}_2\text{O}_3$  est inférieure (37-40 %). La magnétite domine dans certains échantillons, tandis que le clinocllore et la serpentine sont des silicates communs. Les analyses à la microsonde protonique de la chromite provenant des trois types d'échantillons ont révélé des traces de Ni, de Zn et de Ga.

---

\*Chercheur et \*\*technicien en minéralogie, Section de la minéralogie appliquée, Laboratoire de traitement des minéraux, Laboratoires des sciences minérales, CANMET, Énergie, Mines et Ressources Canada, Ottawa (Ontario) K1A 0G1.



## CONTENTS

ABSTRACT .....	i
RÉSUMÉ .....	iii
INTRODUCTION .....	1
ANALYTICAL METHODS .....	1
RESULTS .....	1
PROTON MICROPROBE RESULTS .....	7
DISCUSSION .....	8
Mineralogy of the PGM .....	8
Implications for Mineral Processing .....	8
Spinel Compositions .....	10
Trace Elements .....	10
SUMMARY AND CONCLUSIONS .....	10
ACKNOWLEDGEMENTS .....	11
REFERENCES .....	12

## TABLES

1. Samples studied from the Bird River sill: location and assay values .....	4
9. Proton microprobe analyses of chromite .....	9
10. Relative abundance of PGM in Bird River sill .....	9
11. Summary of PGM found .....	10

## FIGURES

1. Generalized geological setting of the Bird River sill showing location of the Chrome property .....	2
2. Detail of the Chromitiferous Zone with height above base of sill in metres .....	3
3. Igneous stratigraphy of the Bird River sill .....	3
4-66. Photomicrographs of samples .....	14
67. Distribution of PGM species in Upper and Lower Main Chromitites and in Lower Group Pt-bearing unit .....	30
68. Distribution of five PGE for Lower Group Pt-bearing unit .....	31
69. Host minerals for PGM inclusions in Upper and Lower Banded Chromitites and in Lower Group Pt-bearing unit .....	31
70. Chromite compositions plotted on an Al - Cr - Fe <sup>3+</sup> diagram .....	32
71. Chromite compositions plotted on a Cr-2Ti-Al diagram .....	32
72. A plot of Ti vs Cr/(Cr+Al) for the spinel analyses .....	33

**APPENDIX**

Table 2 – Energy dispersive analyses of spinels from Bird River sill samples .....	37
Table 3 – Energy dispersive analyses of silicate minerals from Bird River sill samples .....	41
Table 4 – Electron microprobe analyses of laurite from Bird River sill samples .....	48
Table 5 – Electron microprobe analyses of pentlandite from Bird River sill (sample SEB-84-7) .....	49
Table 6 – Electron microprobe analyses of Pd minerals from Bird River sill samples .....	50
Table 7 – Electron microprobe analyses of sperrylite grains from Bird River sill samples .....	51
Table 8 – Electron microprobe analyses of hollingworthite and Os-Ir-Ru alloy from Bird River sill samples .....	52



## INTRODUCTION

The Bird River sill, located approximately 130 km northeast of Winnipeg, Manitoba, close to the Ontario border, has recently been the focus of investigations concerning the recovery of chromite (Andrews and Jackman, 1987) and the distribution of the platinum-group elements (PGE) (Talkington et al., 1983; Theyer, 1985; Ohnenstetter et al., 1986; Scoates et al., 1987, 1988). The present study was initiated at the request of the Geological Survey of Canada and deals solely with samples collected by GSC personnel from what is known as the Chrome property (Fig. 1). Dr. R.F.J. Scoates, of the Geological Survey of Canada, provided nine hand samples, which are listed in Table 1 together with their locations and PGE assay values for seven of the samples.

The Archean Bird River sill, which is disrupted by numerous cross-faults, contains a Chromitiferous Zone (Fig. 2). It consists of a Lower Ultramafic Series and an Upper Mafic Series (Fig. 3). The sill has a total thickness of about 700 m and a strike length of more than 20 km (Scoates, 1983). The rocks have undergone greenschist facies metamorphism (Cerny et al., 1981). The Ultramafic Series, which consists of five zones, each composed of distinctive lithologic units, is 200 m thick. The Chromitiferous Zone (Fig. 2), which occupies the upper 60 m of the Ultramafic Series (Fig. 3), is composed of alternating peridotite and chromitite layers (Scoates, 1983). Four intervals, containing anomalous PGE concentrations, have been reported from the Ultramafic Series (Scoates et al., in prep.). The interval associated with Lower Group Chromitite (= Lower Group platinum-bearing unit) is reported by Scoates et al. to be the most continuous and the most consistently anomalous. This unit has also been referred to as sulphide-bearing because it contains irregularly disseminated sulphides. Most of the studied samples have come from this unit. Single samples were also studied from each of the two principal chromitite layers occurring stratigraphically above the Lower Group platinum-bearing zone, i.e., the Upper Main Chromitite

and Lower Main Chromitite. These latter samples are from the same general area as those studied by Ohnenstetter et al. (1986) and Talkington et al. (1983). The mineral processing investigation reported by Andrews and Jackman (1988) was carried out on a 70-t sample, which had also been obtained from the Chrome property and included the Upper and part of the Lower Main Chromitite units.

## ANALYTICAL METHODS

All samples were first studied intensively with reflected light microscopy using a 16x objective and a mechanical x-y stage. This was done to ensure that the entire polished surface was examined optically, with special attention to micron-sized platinum-group minerals (PGM). Polished sections of most samples were studied, but many carefully prepared polished thin sections were also examined. To avoid plucking of micron-sized PGM inclusions in soft serpentinized matrix, special attention in sample preparation must be emphasized. Grains of interest, determined with the ore microscope, were marked and further studied with a scanning electron microscope (SEM), which was equipped with an energy dispersive spectrometer (EDS) to identify minerals. Additional quantitative electron microprobe analyses, by wavelength dispersive spectrometry (WDS) of selected grains, were also carried out. Details of standards used and analytical conditions are given under each table. A few proton microprobe (Micro-PIXE) analyses of chromite were also performed. Some of the silicates were identified by X-ray diffraction (XRD) analysis.

## RESULTS

The mineralogy of each sample is described separately to present sufficient relevant details before generalizations and intersample comparisons.

**Sample EI-86-58** Chromite is abundant, as expected, since this sample is from the middle member of the Upper Main Chromitite layer.

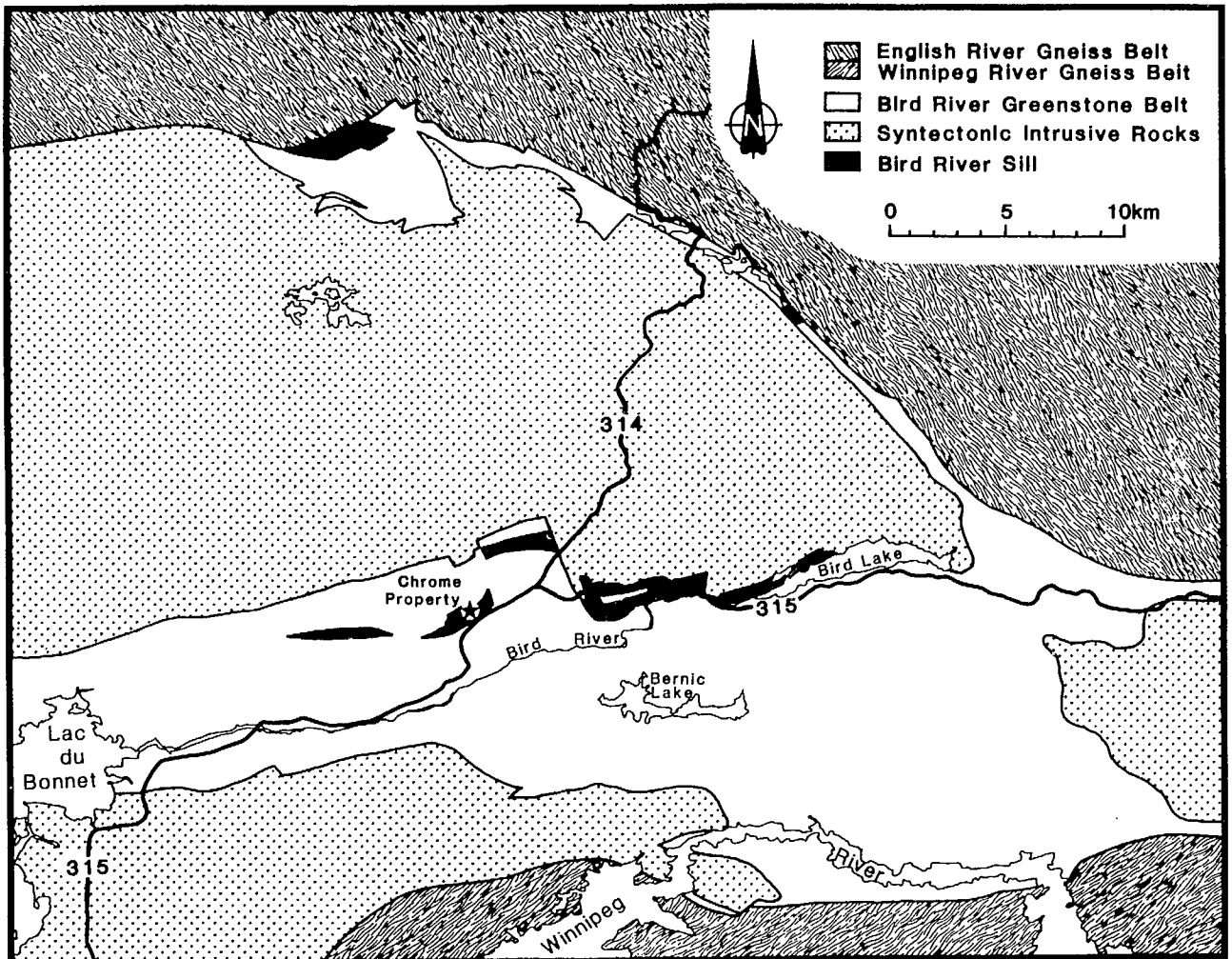


Fig. 1 – Generalized geological setting of the Bird River sill showing location of the Chrome property (from Scoates et al., 1986).

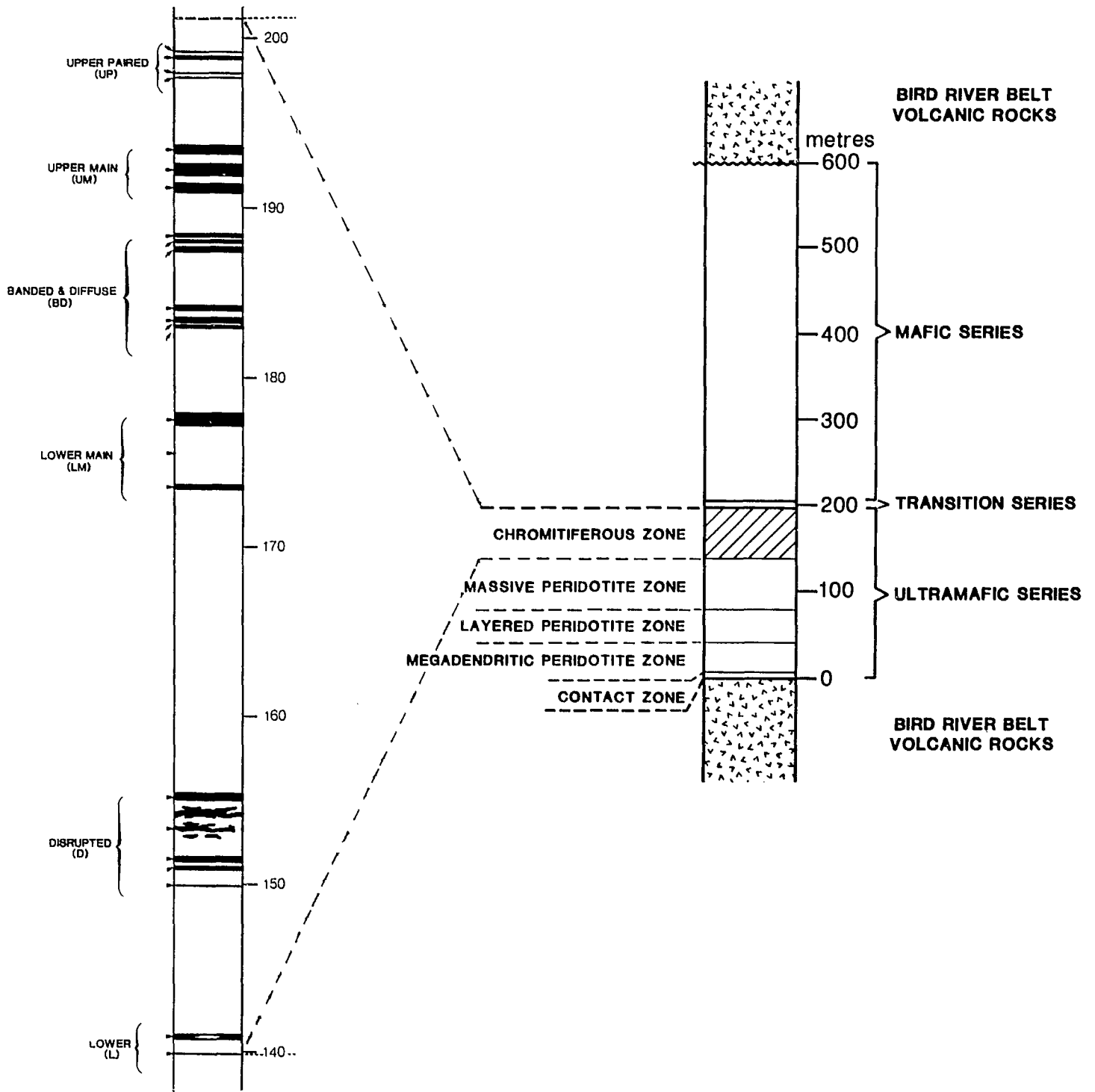


Fig. 2 - Detail of the Chromitiferous Zone, shown on left-hand side, with height above base of sill in metres (from Scoates et al., 1986).

Fig. 3 - Igneous stratigraphy of the Bird River sill, shown on the right-hand side, (from Scoates et al., 1986).

Table 1 – Samples studied from the Bird River sill: location and assay values

Sample Number	Stratigraphic Unit	PGE (ppb)	Pt	Ir	Os	Pd	Rh	Ru	Au
EI-86-58	Upper Main Chromitite, middle member	–	–	–	–	–	–	–	–
SEB-84-15	Lower Main Chromitite	–	–	–	–	–	–	–	–
SEB-84-7	Lower Group Chromitite, Pt-bearing unit 1	2,474	1,800	11	12	480	80	59	32
SEB-85-06	Lower Group Chromitite, Pt-bearing unit 1	1,142	240	76	14	770	40	50	20
SEB-85-07	Lower Group Chromitite, Pt-bearing unit 2	2,004	470	18	4	1,300	86	110	16
SEB-85-10	Lower Group Chromitite, Pt-bearing unit 2	2,154	470	15	16	1,500	69	68	16
SEB-85-16	Lower Group Chromitite, Pt-bearing unit 2	1,622	270	10	17	1,200	46	45	34
SEB-85-18	Lower Group Chromitite, Pt-bearing unit 3	2,003	720	46	62	720	160	290	5
SEB-85-32	Lower Group Chromitite, Pt-bearing unit 5	1,441	562	23	40	550	95	150	23

The Cr content of the chromite is heterogeneous, with patches and irregular rims of higher Cr content (Fig. 4). These high Cr areas appear to be associated with fractures in the chromite matrix and also contain less Al and Mg (Appendix, Table 2, anal. 19). The chromite grains occur in a matrix of clinocllore and grossular (Appendix, Table 3, anal. 28–35). Titanite and lesser amounts of ilmenite are also present in the silicate matrix, whereas millerite (?) occurs either in silicate inclusions in chromite or directly in chromite.

The eight PGM grains found in one polished section consist of six grains of laurite (<1 to 5x14  $\mu\text{m}$ ) and an intergrowth of erlichmanite (0.75x1.5  $\mu\text{m}$ ) and Os–Ir–Ru alloy (1x1.5  $\mu\text{m}$ ). Analyses of four laurite grains are given in the Appendix, Table 4. Three of them (Fig. 5 and 6) and the intergrowth (Fig. 7) are inclusions in chromite, whereas the other three laurite grains are in silicates (Fig. 8). One of the three laurite grains recorded as an inclusion in chromite is actually contained within a 9- $\mu\text{m}$  spherical Mg–Al silicate inclusion in chromite (Fig. 9). Other spherical silicate inclusions are PGM-free. A typical silicate inclusion is shown in Figure 10 and consists of clinocllore (a), mixture (?) (b), Cr–diopside (c) and sphene (d) (Appendix, Table 2, anal. 36–39). The association of chromite-included PGM with high Cr zones may be seen in Figure 5.

**Sample SEB-84-15** The abundant chromite in this sample from the Lower Main Chromitite is very similar texturally (Fig. 11 and 12) and chemically (Appendix, Table 2) to the chromite from the Upper Main Chromitite layers. The chromite grains occur in a matrix consisting principally of clinocllore and grossular. Ni sulphide inclusions are common, many occurring as small grains in chromite at its boundary with silicate.

Of the 16 PGM grains found in one polished section, 11 are laurite grains, ranging between <1 and 4x10  $\mu\text{m}$  in size. Most laurite grains are in the silicate matrix (Fig. 13–17); fewer are in chromite (Fig. 18–20). Analyses of laurite grains are given in Table 4. Also found were three grains (1x2 to 2x3  $\mu\text{m}$ ) of Os–Ir–Ru alloys

(Fig. 21–23 and Appendix, Table 8); all are included in chromite with no apparent alteration or fractures. Finally, one irarsite grain (1x10  $\mu\text{m}$ ), associated with an undetermined PGM containing Pd, Pt, Ru, S, As and Sb, was also found included in silicates.

**Sample SEB-84-7** Magnetite is common in this sample, usually occurring as skeletal intergrowths dispersed throughout the silicate matrix. A few grains of chromite were observed with Fe-rich rims, typical of chromite alteration during serpentinization. Millerite, chalcopyrite, pentlandite, violarite, pyrite and covellite occur in minor to trace amounts, many in contact with, or included within, magnetite. Electron microprobe analyses of millerite revealed that up to 1.5 wt % Fe and 1.0 wt % Co substitute for Ni, and that up to 2.6 wt % Co and 0.60 wt % Ni substitute for Fe in pyrite. Violarite was found to contain up to 8.8 wt % Co. Quantitative analyses of pentlandite (Appendix, Table 5) average 42.3 wt % Ni and 0.69 wt % Co. The high Ni content is consistent with the presence of secondary sulphides, such as violarite and millerite (Harris and Nickel, 1972), and abundant magnetite (probably after pyrrhotite). Pd was sought but was not detected at a minimum detection level of 0.036 wt %.

Only a single grain of merenskyite (5x5  $\mu\text{m}$ ) was found (Fig. 24) despite optical examination of three polished sections and one polished thin section. No Pt-bearing PGM were found in spite of the highest Pt assay value as compared with the other samples that were reported for this sample (Table 1). If the assay is valid, either the PGM distribution is very heterogeneous, or the Pt occurs in solid solution within a mineral or minerals at subdetection levels for the electron microprobe.

**Sample SEB-85-06** Magnetite is the major opaque mineral in this sample, occurring as skeletal intergrowths in a silicate matrix, as in sample SEB-84-07. Chromite grains are characterized by Fe-rich rims. Millerite, chalcopyrite, pentlandite, violarite and pyrite occur in minor to trace quantities and are typically associated with magnetite. This sample shows the possible presence of two generations of violarite: well-polished, smooth-surfaced violarite is usu-

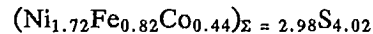
ally indicative of a primary origin, whereas pitted, poorly polished violarite is considered to be an alteration product after pentlandite or pyrrhotite. Two PGM were found in the single polished section examined. One is sperrylite ( $3 \times 7 \mu\text{m}$ ), which is attached to pentlandite and pyrite and extends into silicates (serpentine?), (Appendix, Table 4 and Fig. 25). A single merenskyite grain ( $2 \times 3 \mu\text{m}$ ) was found in pyrite, itself included in pentlandite (Fig. 26).

**Sample SEB-85-07** Chromite, with Fe-rich rims, is the principal opaque mineral in this sample. Another feature of the chromite is its "buckshot" texture, derived from numerous round silicate inclusions, many of them multiminerally (Fig. 27). Electron microprobe analyses of several chromite grains are given in the Appendix, Table 2, and analyses of silicate minerals, occurring either as inclusions in chromite or as matrix to the chromite, are given in the Appendix, Table 3. Sulphide minerals (millerite, violarite, pentlandite, pyrite and chalcopyrite) are present only in trace amounts, many occurring as small inclusions at the chromite/silicate boundary.

Thirteen PGM grains, dominated by the Pd minerals merenskyite and kotulskite, were found in two polished sections (Appendix, Table 6). The three merenskyite grains are relatively large ( $10 \times 20$ ,  $5 \times 11$  and  $2 \times 20 \mu\text{m}$ ), whereas the seven kotulskite grains range from  $1 \times 1$  to a maximum of  $11 \times 30 \mu\text{m}$  (Fig. 28-30). The other three PGM are sperrylite grains ( $2 \times 2$ ,  $8 \times 18$  and  $10 \times 13 \mu\text{m}$ ), shown in Figures 31 and 32. Two sperrylite analyses are given in Table 8. All these PGM inclusions, as in the previous sample, are either hosted by, or in contact with, sulphide minerals (pyrite, pentlandite or violarite), themselves enclosed by silicates. Qualitatively, there is good correlation between assay values (Table 1) and the nature of PGM found.

**Sample SEB-85-10** Magnetite is the principal opaque mineral, occurring as massive segregations, as rims to chromite remnants, or as disseminations in silicates. It covers roughly one third, by area, of the sections studied optically. Ilmenite occurs in minor to trace amounts as inclusions in magnetite. A few laths of barite

were found in the silicates. The sulphide minerals (millerite, pentlandite, violarite, pyrite and chalcopyrite) are extremely sparse, occurring as fine-grained inclusions mainly in silicates but also in magnetite, often as multiminerally composite grains. One violarite grain is sufficiently large for a quantitative WDS analysis, resulting in the formula:



Thirteen PGM, representing a diverse suite of minerals, were found by optical examination of four polished sections and one polished thin section. Five are Pd minerals (four keithconite  $1 \times 1$  to  $2 \times 4 \mu\text{m}$  and one mertieite II  $1.5 \times 2 \mu\text{m}$ ); four are the Rh mineral hollingworthite ( $1.5 \times 1.5$  to  $4 \times 8 \mu\text{m}$ ), often exhibiting considerable Pt substitution for Rh; three are sperrylite ( $2 \times 4$  to  $3 \times 4 \mu\text{m}$ ), and one is a single grain of laurite ( $1 \times 1 \mu\text{m}$ ). Most of these PGM (nine grains) are enclosed in silicates (Fig. 33-35); three occur at the magnetite/silicate boundary (Fig. 36 and 37); and one sperrylite grain is included in magnetite (Fig. 38). Correlation of PGE assay values (Table 1) with the PGM found also appears quite good qualitatively.

**Sample SEB-85-16** Chromite is the major opaque mineral in this sample (an estimated 25-30% of the whole sample) occurring as two cumulus layers. The chromite generally has Fe-rich rims (Fig. 39), and some grains have an intergrowth texture with the silicates reminiscent of a corroded or replacement (recrystallized?) texture. This texture is more common in sample SEB-85-18. Magnetite is also present as a minor constituent occurring as skeletal disseminations in silicate. The sulphides (millerite > violarite > chalcopyrite, pentlandite and pyrite) are generally present as fine-grained disseminations in silicate. However, a few large millerite grains were observed (up to  $360 \mu\text{m}$  in maximum dimension). A few small multiminerally sulphide grains also occur in chromite.

Nine laurite grains were the sole PGM species found during optical examination of two polished sections. The grains range from  $1 \times 1$  to  $5 \times 8 \mu\text{m}$ ; seven of the grains occur as inclusions

in silicate (e.g., Fig. 40) and two in chromite (Fig. 41 and 42).

Despite a relatively high assay value of 1200 ppb Pd, no Pd minerals were identified. On the other hand, some laurite grains were found, despite the low assay value of 45 ppb Ru for the sample. The PGM found do not correlate well with the assays, as was determined for sample SEB-84-7.

**Sample SEB-85-18** This sample contains abundant cumulus chromite, having a pronounced corroded (recrystallized?) texture (Fig. 43), as is present in sample SEB-85-16. Qualitative EDS analyses indicated that the silicate intergrowths found within the chromite were the same as the host matrix. The matrix silicate was confirmed to be clinocllore by X-ray powder diffraction. Numerous sulphides (violarite, millerite, pentlandite, pyrite and chalcopyrite) occur within the chromite, usually as multimineralic grains.

Fifty-four PGM grains were found (in only two polished sections), and all are inclusions in the silicate matrix. Eighteen are laurite grains (Appendix, Table 4 and Fig. 44-49), which range in size from 1x1 to 6x9  $\mu\text{m}$ . Seventeen sperrylite grains were identified (Appendix, Table 7) and range in size from 1x2 to 10x15  $\mu\text{m}$  (Fig. 49-54). Eight grains of keithconnite (Appendix, Table 6) were identified (Fig. 55 and 56), half of which are attached to sperrylite (Fig. 52-54). The keithconnite grains range in size from 1x1 to 4x6  $\mu\text{m}$  and probably represent only the second reported occurrence of the mineral since its original characterization in the J-M reef of the Stillwater Complex, Montana (Cabri et al., 1979). Six grains of irarsite were also identified, ranging in size from <1 to 2x2  $\mu\text{m}$  (Fig. 47 and 48) as well as three grains of hollingworthite (1x2, 1.5x2 and 2x3  $\mu\text{m}$ ) (Fig. 55). One hollingworthite grain is attached to sperrylite and a second is attached to laurite (Fig. 57). Finally, two unidentified PGM (1x2 and 10x10  $\mu\text{m}$ ), possibly consisting of fine-grained intergrowths, were also observed. Qualitative EDS analyses of the unidentified grains indicate that they contain Pd, Te, Mn, Ni and Cu. The diversity of PGM found, representing Pt, Pd,

Ru, Rh and Ir minerals, correlates fairly well with the assay values (Table 1).

**Sample SEB-85-32** A study of four polished sections reveals that the chromite and magnetite content of this sample is variable. Chromite displays typical Fe-rich rims and some grains contain rounded silicate inclusions, usually near grain centres. Magnetite, a minor constituent, occurs principally as a replacement of chromite, but is also intergrown with sulphides. The sulphides (millerite, violarite, pentlandite, pyrite and chalcopyrite) generally occur as small multi-mineralic inclusions in either chromite or silicate, and most are intergrown with magnetite. Sulpharsenides (cobaltite and gersdorffite), generally intergrown with sulphides, occur as small inclusions in chromite or in silicates.

Eighteen PGM grains were found, including six laurite grains (Appendix, Table 4), which range in size between 1x3 and 7x12  $\mu\text{m}$ . Four laurite grains occur in silicates and two in chromite (Fig. 58 and 59). Four sperrylite grains were identified (Appendix, Table 7), ranging in size from 1x2 to 8x9  $\mu\text{m}$ ; all are included in silicate (Fig. 60-62). Four grains of merenskyite (1x1 to 3x6  $\mu\text{m}$ ) were identified: two in silicate (Fig. 62), one in magnetite (Fig. 63) and one in millerite, in contact with silicate (Fig. 64). Two hollingworthite 2.5x3  $\mu\text{m}$  grains were identified; one is attached to pentlandite (?) in silicate (Appendix, Table 8 and Fig. 65), and the other is attached to laurite (Fig. 66), which is in contact with a grain of keithconnite (Appendix, Table 6). All these grains are included in silicate. Finally, a single grain of mertieite II was identified (Appendix, Table 6), occurring as a 6x12- $\mu\text{m}$  inclusion in silicate (Fig. 63). Correlation between the PGM found and the assay values (Table 1) is fairly good.

## PROTON MICROPROBE RESULTS

Five chromite grains were analyzed with a proton microprobe at the Max Planck Institut für Kernphysik, Heidelberg, West Germany. The grains are from the Upper and Lower Main Chromitites as well as from the Lower Group

platinum-bearing unit. The trace contents of Ni, Zn and Ga are somewhat similar, but Ni seems to increase with stratigraphic depth (Table 9). Too few analyses were undertaken to be sure of any definitive trend.

## DISCUSSION

### Mineralogy of the PGM

The PGM suite of the Upper Main Chromitite and the Lower Main Chromitite is in marked contrast to all samples from the Lower Group Chromitite, except for one (SEB-85-16). The PGM found in the sulphide-poor chromite-rich Upper and Lower Main Chromitites are almost exclusively (96%) represented by minerals of Ru, Ir and Os (Table 10). In contrast, the Pt-bearing member of the Lower Group Chromitite contains a more diverse suite of PGM, including Pt, Pd and Rh as well as Ru and Ir, and may be described as relatively sulphide-rich. Os is represented by substitutions in other PGM, especially laurite (Appendix, Table 5). The difference between the PGM in the two suites is shown graphically in Figure 67 by means of their vol % [calculated on length and width  $\times$  1/2 (length + width)].

The PGM suite found in the Upper and Lower Main Chromitites is in very good agreement with that reported by Talkington et al. (1983) and Ohnenstetter et al. (1986). The PGM identified in these chromitites are also consistent with the Ru-dominant assays for  $\text{Cr}_2\text{O}_3$ -rich samples reported by Talkington and Watkinson (1986).

Comparison between the PGM found and assay values is an indication of whether or not the PGM are representative of all the PGE values. Such a comparison is very difficult to achieve on a quantitative basis in practice, as there are usually too few PGM in each polished section to provide a statistically reliable grain count. This handicap may be overcome, to a certain degree, where the PGM grains are large enough for concentration before examination in a polished section (e.g., Cabri and Laflamme, 1984). The

PGM in the Bird River samples are too fine-grained, and since they are commonly included in a soft mineral (clinocllore), it is difficult to produce a good representative polished section without losing some PGM grains during polishing. Therefore, comparisons between PGM found and assay results are qualitative only. A summary of the number of PGM found and the number of polished sections and polished thin sections examined is given in Table 11.

Another way to compare the mineralogical findings with the assays is to calculate the mass for each PGE from the vol % data. This was done for all PGE except Os, assuming ideal compositions for the PGM found in the Lower Group platinum-bearing unit. The results of PGE distribution are compared with the average assay PGE distribution (Table 1) in Figure 68. The correspondence between the PGE distribution calculated from PGM and from the assays is very close. In fact, the largest discrepancies may also be partly due to known substitutions of Rh for Pt in sperrylite, Rh for Ir in irarsite, and Ir and Pt for Rh in hollingworthite.

### Implications for Mineral Processing

The size of PGM inclusions and their host mineral are important considerations for mineral processing. In general terms, the size of PGM in the chromitite bands (Upper and Lower Main) and in the Lower Group platinum-bearing unit are comparable, with most grains being 5  $\mu\text{m}$  or less in largest dimension. However, grains up to 30  $\mu\text{m}$  were observed in the Lower Group platinum-bearing zone, in comparison with 14  $\mu\text{m}$  as the largest found in the two chromitites. On the other hand, the distribution of PGM in their host mineral is considerably different if those two stratigraphic environments are compared, as shown graphically in Figure 69. In addition, the results for PGM inclusions in the Upper and Lower Main Chromitites are in conflict with the data of Ohnenstetter et al. (1986), who reported only a single PGM *not* included in chromite (in about 100 specimens) from the Upper Main Chromitite.



Table 9 – Proton microprobe analyses of chromite (ppm)

Sample No.	Grain	Ni	Zn	Ga
EI-86-58 (U.M.)	1	921 ± 34	501 ± 13	71 ± 7
EI-86-58 (U.M.)	2	873 ± 46	521 ± 18	48 ± 9
SEB-84-15 (L.M.)	1	1,381 ± 43	509 ± 16	57 ± 8
SEB-84-15 (L.M.)	2	1,310 ± 43	503 ± 16	60 ± 7
SEB-85-32 (L.G.)	1	1,802 ± 41	678 ± 15	81 ± 7

Analyses were done with a 200 µm Al absorber at 4 MeV. The beam integrated charge was about 0.27 µC on a 5x6 µm area for about 30 minutes. The analyses were computed using similar methods and synthetic standards to those reported by Cabri et al. (1985).

Table 10 – Relative abundance of PGM in Bird River sill

	Common	Less common	Rare to very rare
Upper Main Chromitite	laurite (RuS <sub>2</sub> )*	–	Os-Ir-Ru alloy erlichmanite (OsS <sub>2</sub> )
Lower Main Chromitite	laurite (RuS <sub>2</sub> )	Os-Ir-Ru alloy	irarsite (IrAsS) UK (Pd,Pt,Ru,S,As,Sb)
Lower Group Chromitite (Pt-bearing members)	sperrylite (PtAs <sub>2</sub> ) laurite (RuS <sub>2</sub> )	kotulskite (PdTe) merenskyite (PdTe <sub>2</sub> ) hollingworthite (RhAsS) keithconnite (Pd <sub>3-x</sub> Te) irarsite (IrAsS)	mertieite II (Pd <sub>8</sub> Sb <sub>3</sub> ) UK (Pd,Te,Mn,Ni,Cu)

\*ideal formula, given only for named minerals

Table 11 - Summary of PGM found

Sample	No. polished sections	No. PGM grains
EI-86-58	1	8
SEB-84-15	1	16
SEB-84-7	4*	1
SEB-85-06	1	2
SEB-85-07	2	13
SEB-85-10	5*	13
SEB-85-16	2*	9
SEB-85-18	2*	54
SEB-85-32	4	18

\*includes one polished thin section

### Spinel Compositions

Electron microprobe analyses of spinel are plotted on a Cr-Al-Fe<sup>3+</sup> diagram (Fig. 70) and show, for example, the effect of Al loss and Fe<sup>3+</sup> gain in the alteration rims. The major cluster of analyses is due to the relatively unaltered core zones, which contain analyses from all three zones examined in this study. Both core and rim analyses correspond to the data of Ohnenstetter et al. (1986) for Upper Main Chromitite. The chromite compositions from core areas project onto the field of stratiform intrusions. However, the two analyses representing the Cr-rich zones have not been recorded in the literature\* and may represent the results of a different type of reaction to that which caused the Cr-depleted rims.

With one exception, Ti-rich chromites reported by Ohnenstetter et al. (1986) were not found (Fig. 71). Eales and Reynolds (1983) interpreted the Ti trend to be due to magmatic fractionation. The lack of a Ti-rich chromite trend may also be seen in the form of a Ti vs Cr/(Cr+Al) plot (Fig. 72), again, with the exception of one data point.

### Trace Elements

The few proton microprobe analyses of chromite that were performed reveal trace contents of Ga which are comparable to the 80 ppm obtained for eight chromite samples from Greece, by spark-source-mass spectrometry (Agiorgitis et al., 1976) and to the single proton microprobe analysis of 70 ppm on a chromite of unknown origin, reported by Sie and Ryan (1986). Though Ga concentration in chromite is not widely known, the recent experimental work of Malvin and Drake (1987) demonstrates that Ga is highly compatible in spinel [D(Ga) = 4.6] in contrast to its incompatibility in forsterite and diopside [D(Ga) = 0.024 and 0.19, respectively], and its slight incompatibility in anorthite [D(Ga) = 0.86]. The mechanism for Ga substitution is presumed to be the direct replacement of Al<sup>3+</sup>, which is present in most chromites.

## SUMMARY AND CONCLUSIONS

The results of a preliminary investigation of the mineralogy and the mineralogical distribution of the PGE in samples from the Chrome property, Bird River sill, may be summarized as follows:

\*Note added in proof. Shen et al. (1988) report texturally similar Cr-rich zones from a podiform chromitite deposit.

1. Three textural/chemical varieties of chromite were found:
  - a. chromite with cores containing about 37–40%  $\text{Cr}_2\text{O}_3$  and relatively regular alteration rims with about 31–36%  $\text{Cr}_2\text{O}_3$ . This chromite occurs in the Lower Group platinum-bearing member, units 1, 2 and 5.
  - b. chromite with a corroded (recrystallized ?) texture occurs in the Lower Group platinum-bearing member, units 2 and 3.
  - c. chromite with a higher  $\text{Cr}_2\text{O}_3$  content (43–46%), also containing irregular patches and rims of higher  $\text{Cr}_2\text{O}_3$  (57–58%), occurs in the Upper and Lower Main Chromitites.
2. Chromites from all three stratigraphic horizons contain trace quantities of Ni, Zn and Ga.
3. The number of PGM species found in both the Upper and Lower Main Chromitites (3) is considerably fewer than that found in the Lower Group platinum-bearing unit (9). The distribution of PGE, calculated from assay data, agrees fairly well with that calculated from the mineralogical study. This suggests that the PGM found are probably representative of the samples studied.
4. The host-mineral distribution for PGM inclusions varies markedly between the Lower Group platinum-bearing unit and that found in the Upper and Lower Main Chromitites. The former should be more amenable to recovery of a by-product PGE concentrate because a greater proportion of the PGM is included in, or attached to, silicates and sulphides (Merkle, 1987; Overbeek et al., 1985; Von Gruenewaldt and Hatton, 1987).

The core-to-rim decrease in  $\text{Cr}_2\text{O}_3$  content for the first variety of chromite is accompanied by an even larger decrease in  $\text{Al}_2\text{O}_3$  and a similar decrease in  $\text{MgO}$ , together with substantial increases in  $\text{FeO}$  and  $\text{Fe}_2\text{O}_3$ . Interestingly, these correlations do not appear in analyses of the third variety of chromite. In this case, a decrease in  $\text{Cr}_2\text{O}_3$  content is accompanied by an *increase* in  $\text{Al}_2\text{O}_3$ ,  $\text{Fe}_2\text{O}_3$  and  $\text{MgO}$  and a *decrease* in  $\text{FeO}$ . No Ti trend was observed in chromites analyzed.

## ACKNOWLEDGEMENTS

We are grateful for the encouragement and help provided by Drs. R.F.J. Scoates and O.R. Eckstrand of the Geological Survey of Canada.

## REFERENCES

- Agiorgitis, G., Panagos, A. and Marian, R. "Bestimmung einiger seltener Elemente in griechischen Chromiten"; *Chem Erde*; Bd 35 S; 199-201; 1976.
- Andrews, P.R.A. and Jackman, I. "Laboratory and pilot-plant beneficiation of chromite ore from Bird River, Manitoba"; *Can Min Metall Bull* 81, No. 912; 40-48; 1988.
- Cabri, L.J. and Laflamme, J.H.G. "Mineralogy and distribution of platinum-group elements in mill products from Sudbury"; *Proc Second Int Congress on Applied Mineralogy*; (edited by W.C. Park, D.M. Hausen and R.D. Hagni); Los Angeles; 911-922; 1984.
- Cabri, L.J., Campbell, J.L., Laflamme, J.H.G., Leigh, R.G., Maxwell, J.A. and Scott, J.D. "Proton microprobe analysis of trace elements in sulfides from some massive sulfide deposits"; *Can Mineral* 23; 133-148; 1985.
- Cabri, L.J., Rowland, J.F., Laflamme, J.H.G. and Stewart, J.M. "Keithconnite, telluropalladinite and other Pd-Pt tellurides from the Stillwater Complex, Montana"; *Can Mineral* 17; 589-594; 1979.
- Cerny, P., Trueman, D.L., Ziehlke, D.V., Goad, B.E. and Paul, B.J. "The Cat Lake - Winnipeg River and the Wekusko Lake pegmatite fields, Manitoba"; *Econ Geol Rep* ER80-1; 1-240; Manitoba Mineral Res Div; 1981.
- Eales, H.V. and Reynolds, I.M. "Factors affecting the composition of chromite and magnetite in some southern African rocks"; *Spec Publ Geol Soc S Africa* 7; 5-20; 1983.
- Harris, D.C. and Nickel, E.H. "Pentlandite compositions in some mineral deposits"; *Can Mineral* 11; 861-878; 1972.
- Malvin, D.J. and Drake, M.J. "Experimental determination of crystal/melt partitioning of Ga and Ge in the system forsterite-anorthite-diopside"; *Geochim Cosmochim Acta* 51; 2117-2128; 1987.
- Merkle, R.K.W. "Estimation of recovery characteristics for the platinum-group elements in chromitite layers underlying the UG-2 in the Bushveld complex"; *5th Magmatic Sulphides Field Conference*, IGCP Project 161, Abstr & Field Guide; edited by A. Campbell; Harare; 18; 1987.
- Ohnenstetter, D., Watkinson, D.H., Jones, P.C. and Talkington, R.W. "Cryptic compositional variation in laurite and enclosing chromite from the Bird River sill, Manitoba"; *Econ Geol Rep* 81; 1159-1168; 1986.
- Overbeek, P.W., Loo, J.P. and Dunne, R.C. "The development of a concentration procedure for the platinum-group metals and chromite from the UG-2 Reef of the Bushveld Complex"; *Symp on Precious Metals Recovery*; Miller Freeman Publications, San Francisco; 1985.
- Scoates, R.F.J. "Preliminary stratigraphic examination of the ultramafic zone of the Bird River sill, Manitoba"; *Report of Field Activities*; 70-83; Manitoba Mineral Res Div; 1983.
- Scoates, R.F.J., Eckstrand, O.R. and Cabri, L.J. "Interelement correlation, stratigraphic variation and distribution of PGE in the ultramafic zones of the Bird River sill, Canada"; *Geo-Platinum 87 Symposium*, Abstract F-1; Milton Keynes; 1987.
- Scoates, R.F.J., Eckstrand, O.R. and Cabri, L.J. "Interelement correlation stratigraphic variation and distribution of PGE in the ultramafic zones of the Bird River sill, Canada"; *Proc Geo Platinum 87*; edited by H.M. Prichard, R.J. Potts, J.F.W. Bowles

- and S.J. Cribb; Barking, England, Elsevier; 239-249; 1988.
- Scoates, R.F.J., Williamson, B.L., Duke, J.M., Mandziuk, W., Brisbin, W.C. and Sutcliffe, R.H. "Layered intrusions of southeastern Manitoba and northwestern Ontario"; In Field Trip 13: Guide book, GAC/MAC/CGU Annual Meeting, May 21-24; 1986.
- Shen, P., Hwang, S.-L., Chu, H.-T. and Jeng, R.-C. "STEM study of 'ferritchromit' from the Heng-Chun chromitite"; *Am Mineral* 73; 383-388; 1988.
- Sie, S.H. and Ryan, C.G. "An electrostatic 'Russian' quadruplet microprobe lens"; *Nucl Instr Methods* B16; 664-668; 1986.
- Talkington, R.W. and Watkinson, D.H. "Whole rock platinum-group element trends in chromite-rich rock in ophiolitic and stratiform igneous complexes"; In: *Symp on Metallogeny of Basic and Ultrabasic Rocks*; edited by M.J. Gallagher, R.A. Ixer, C.R. Neary and H.M. Prichard; Inst Mining Metallurgy, London; 427-440; 1986.
- Talkington, R.W., Watkinson, D.H., Whittaker, P.J. and Jones, P.C. "Platinum-group-mineral inclusions in chromite from the Bird River sill, Manitoba"; *Miner Deposita* 18; 245-255; 1983.
- Theyer, P. "Platinum-group elements in the Bird River sill"; 4th Internat Platinum Symposium, Toronto; Abstract, *Can Mineral* 23; 316-317; 1985.
- Von Gruenewaldt, G. and Hatton, C.J. "Platinum-group metals - a resource in the tailings of chromium mines in South Africa"; *J S Afr Inst Min Metall* 87; 265-268; 1987.



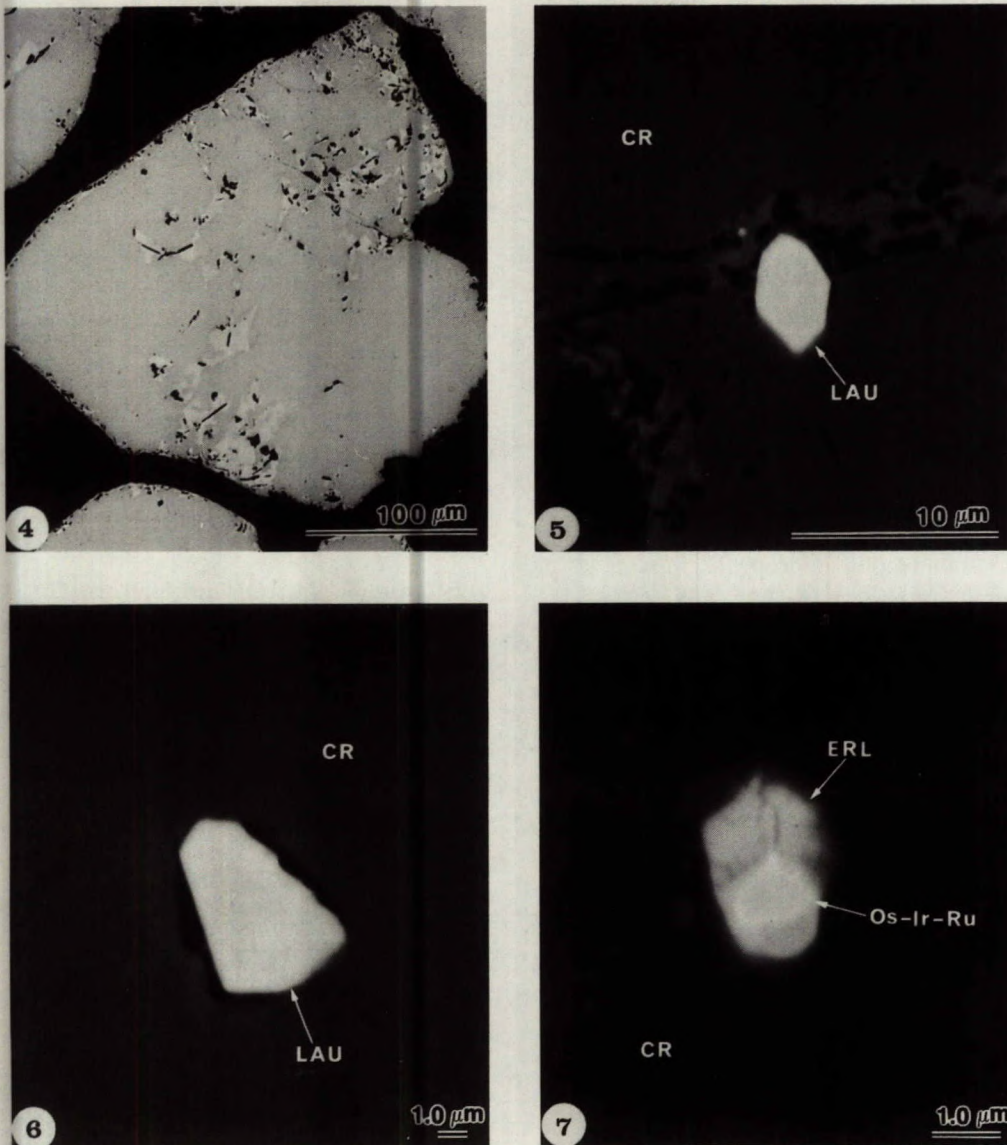


Fig. 4 – Backscattered electron image (BEI) showing areas (lighter grey) with higher Cr and lower Al and Mg contents. Sample EI-86-58.

Fig. 5 – SEM photomicrograph of a euhedral laurite (LAU) grain (Appendix, Table 4, anal. 1) included in chromite (CR) (Appendix, Table 2, anal. 18, 19). Sample EI-86-58.

Fig. 6 – SEM photomicrograph of a subhedral laurite (LAU) grain (Appendix, Table 4 anal. 2) included in chromite (CR) (Appendix, Table 2, anal. 17). Sample EI-86-58.

Fig. 7 – SEM photomicrograph of an intergrowth of Os-Ir-Ru alloy (white) with fractured erlichmanite (ERL), both included in chromite (CR) (Appendix, Table 2, anal. 22). The erlichmanite occurs alongside a fracture (upper left) that extends to the silicate matrix (outside the area shown). Sample EI-86-58.



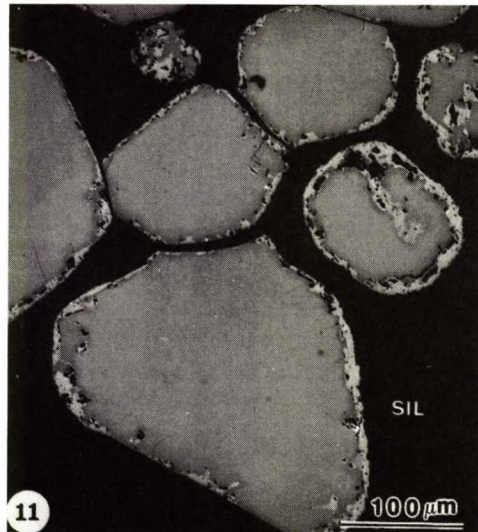
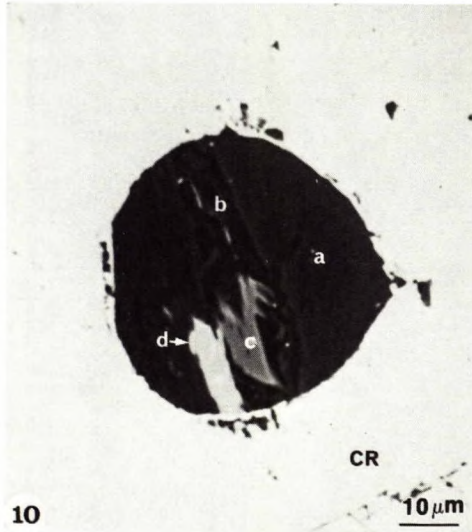
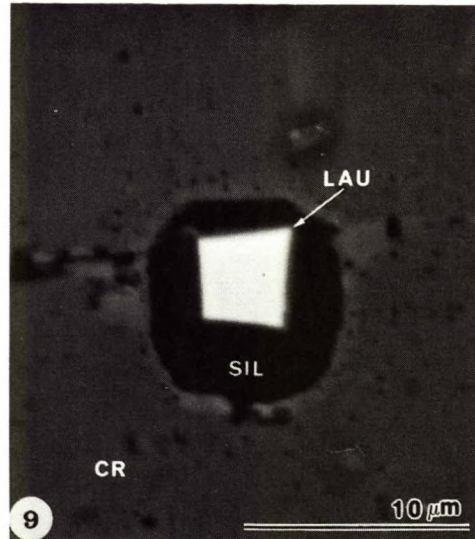
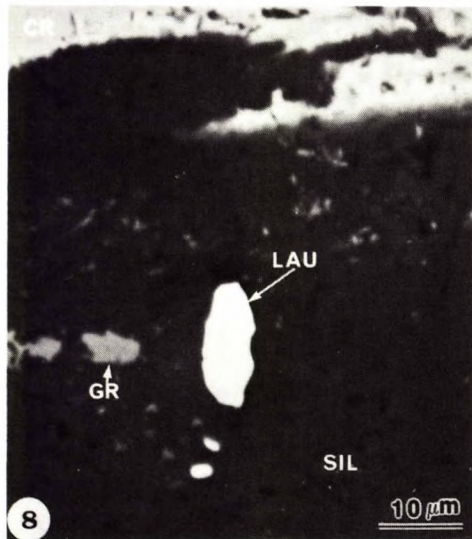


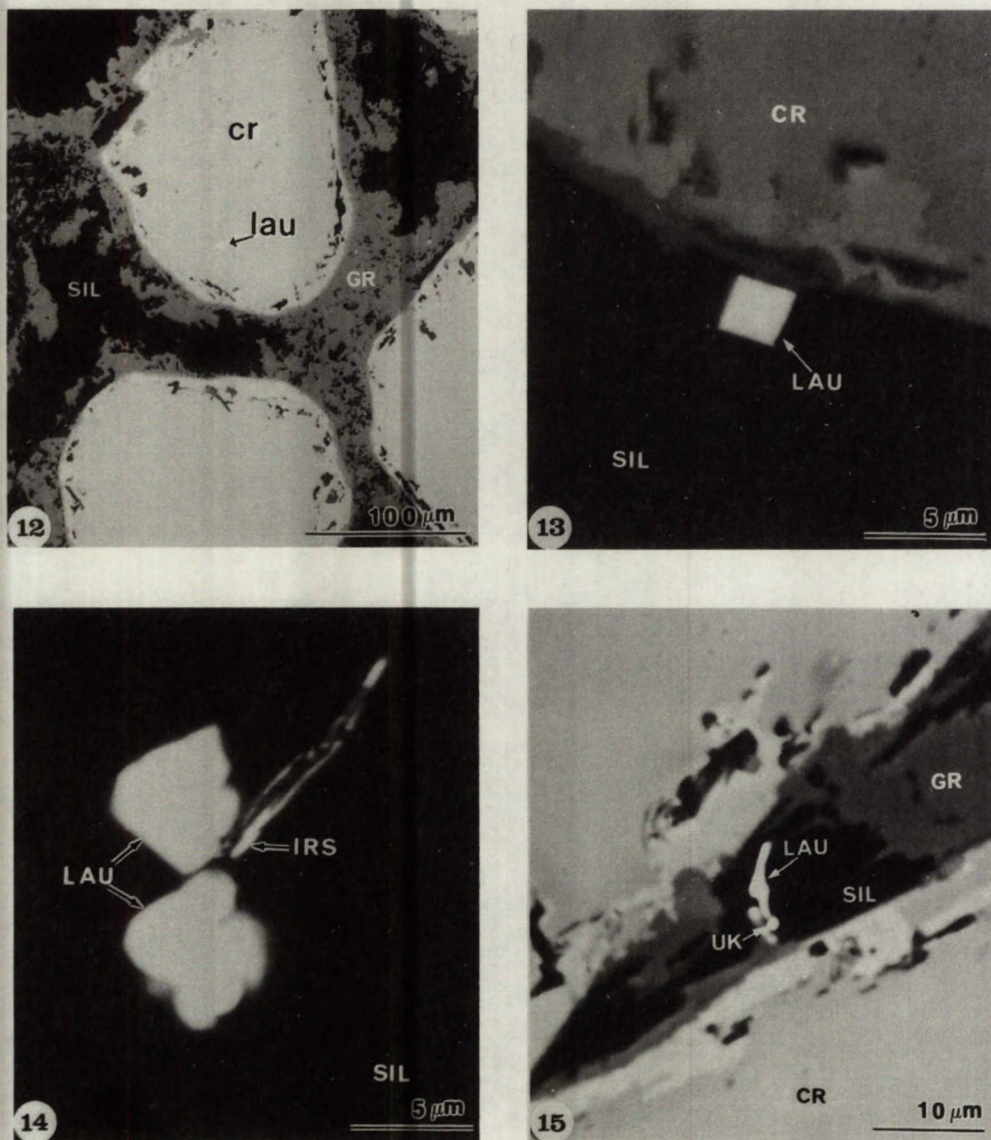
Fig. 8 – SEM photomicrograph showing three anhedral white laurite (LAU) grains (Appendix, Table 4, anal. 3) in clinochlore (?) (SIL) (Appendix, Table 3, anal. 33) with some grossular (GR) grains (Appendix, Table 3, anal. 34), medium grey, left of laurite. Chromite is present in the upper part. Sample EI-86-58.

Fig. 9 – SEM photomicrograph of a euhedral laurite (LAU) grain (Appendix, Table 4, anal. 4) enclosed in clinochlore (?) (SIL) (Appendix, Table 3, anal. 40) in chromite (CR) (Appendix, Table 2, anal. 21). A zone of high Cr (and lower Al and Mg) is seen as a rim (light grey) to the silicate inclusion and extending left and right. Sample EI-86-58.

Fig. 10 – SEM photomicrograph of a composite silicate inclusion (Appendix, Table 3, anal. 37-39) in chromite similar in composition to analyses 21 and 22, Table 2. Sample EI-86-58.

Fig. 11 – BEI photomicrograph showing cumulus chromite grains with typical Cr-rich rims. Sample SEB-84-15.





- Fig. 12 – SEM photomicrograph of several chromite (CR) grains (Appendix, Table 2, anal. 29) with light-coloured Cr-rich rims enclosed by grossular (GR) and clinocllore (?). A laurite (LAU) inclusion may be seen in one chromite, details of which are given in Figure 18. Sample SEB-84-15.
- Fig. 13 – SEM photomicrograph of a euhedral laurite (LAU) grain in clinocllore (?) (SIL) (Appendix, Table 3, anal. 53) nearly in contact with chromite (CR). Sample SEB-84-15.
- Fig. 14 – SEM photomicrograph of two subhedral laurite (LAU) grains with a lath of irarsite (IRS) in clinocllore (?) (SIL) (Appendix, Table 3, anal. 50). Sample SEB-84-15.
- Fig. 15 – SEM photomicrograph of a subhedral laurite (LAU) grain with a smaller (Pd, Pt, Ru, S, As, Sb) inclusion (UK) in contact with grossular (GR) (Appendix, Table 3, anal. 52) enclosed in clinocllore (?) (SIL) (Appendix, Table 3, anal. 51) between chromite (CR) grains. Sample SEB-84-15.



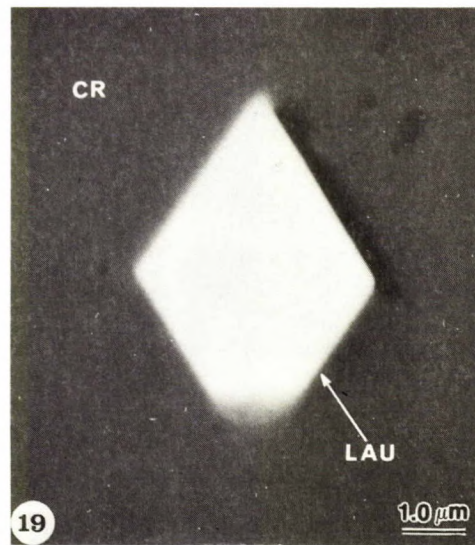
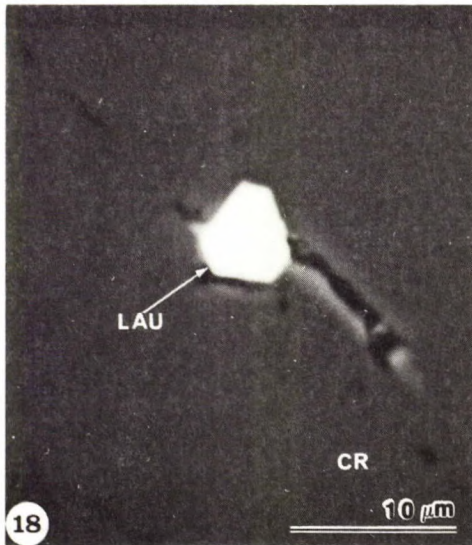
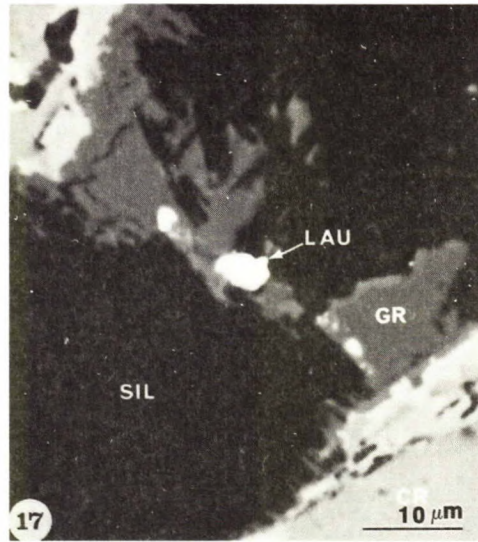
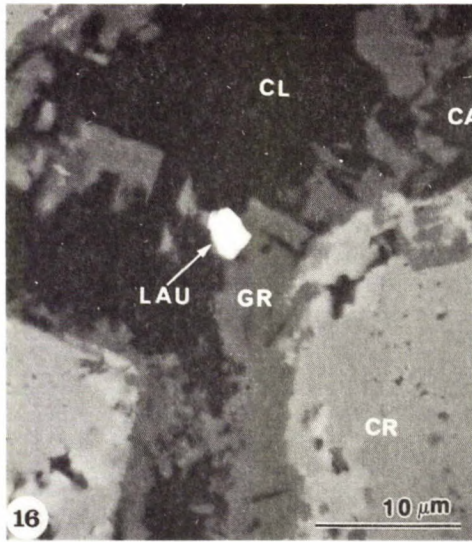


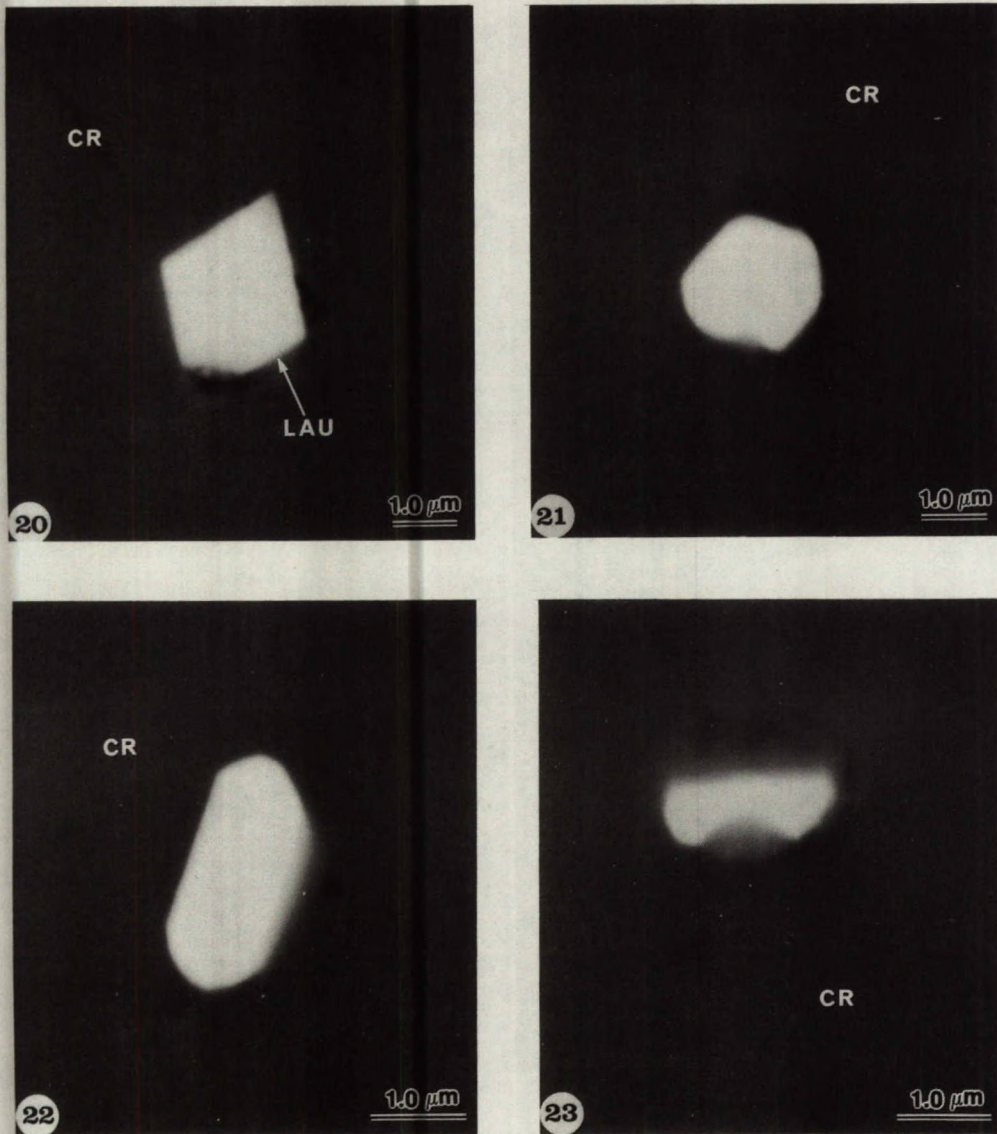
Fig. 16 – SEM photomicrograph of an anhedral laurite (LAU) grain (Appendix, Table 4, anal. 7) in contact with grossular (GR) (Appendix, Table 3, anal. 48) and clinocllore (?) (CL) (Appendix, Table 3, anal. 49) between chromite grains showing Cr-rich areas. Calcite (CA) is present in the upper right. Sample SEB-84-15.

Fig. 17 – SEM photomicrograph of three anhedral laurite (LAU) grains included in grossular (GR) (Appendix, Table 3, anal. 46), itself included in clinocllore (?) (SIL) (Appendix, Table 3, anal. 47), occurring between chromite grains as in Figure 13. Sample SEB-84-15.

Fig. 18 – SEM photomicrograph of the same laurite (LAU) grain enclosed in chromite (CR) shown in Figure 12. The laurite straddles a microfracture in the chromite, which is also associated with Cr-rich areas.

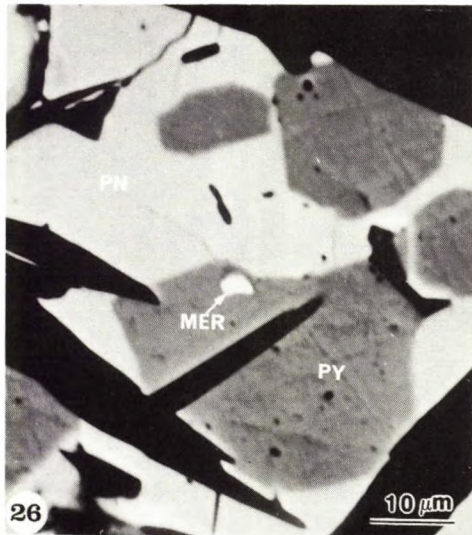
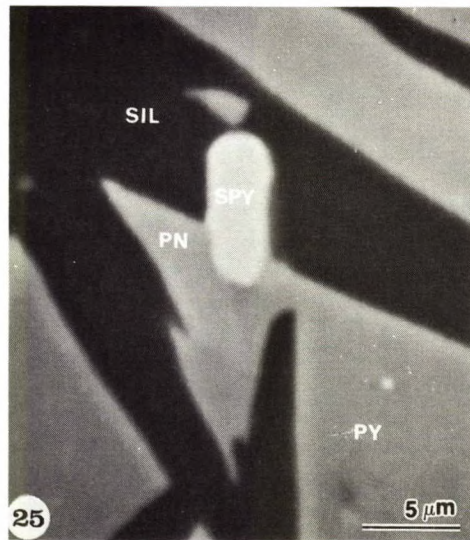
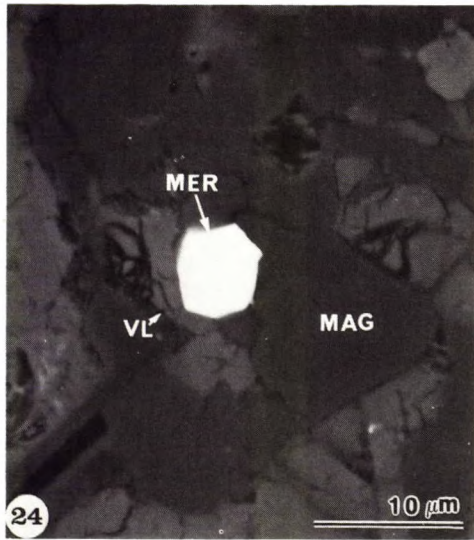
Fig. 19 – SEM photomicrograph of a euhedral laurite (LAU) grain included in chromite (CR). Compare to Figure 18. Sample SEB-84-15.





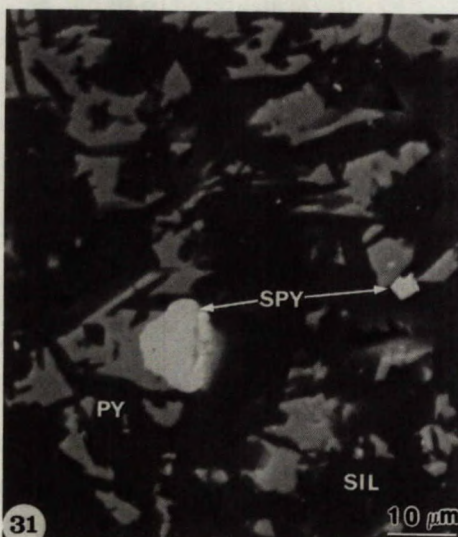
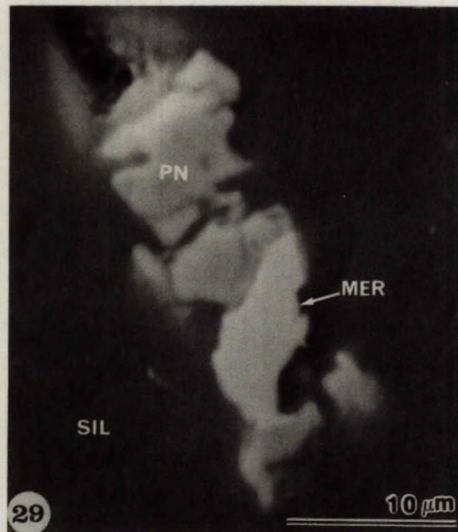
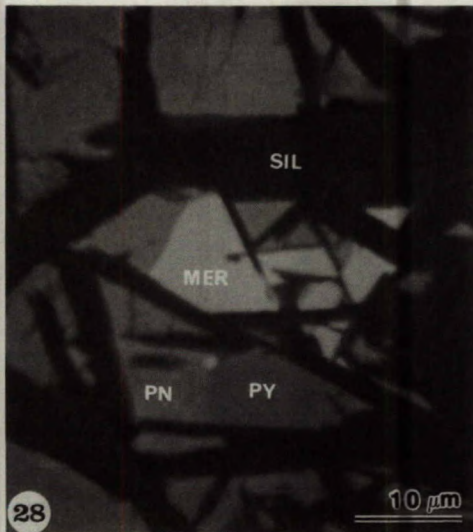
- Fig. 20 - SEM photomicrograph of another euhedral laurite (LAU) grain included in chromite (CR) (Appendix, Table 2, anal. 28) related to an incipient fracture (?). Sample SEB-84-15.
- Fig. 21 - SEM photomicrograph of a subhedral grain of rutheniridosmine (Appendix, Table 8) included in chromite (CR). Sample SEB-84-15.
- Fig. 22 - SEM photomicrograph of a euhedral platelet of Os-Ir-Ru alloy included in chromite (CR) (Appendix, Table 2, anal. 27). Sample SEB-84-15.
- Fig. 23 - SEM photomicrograph of an anhedral grain of Os-Ir-Ru alloy included in chromite (CR) (Appendix, Table 2, anal. 31). Sample SEB-84-15.





- Fig. 24 – SEM photomicrograph of a merenskyite (MER) inclusion in magnetite (MAG) and attached to violarite (VL) which has shrinkage cracks. Sample SEB-84-7.
- Fig. 25 – SEM photomicrograph of a tabular sperrylite (SPY) inclusion in pentlandite (PN), pyrite (PY) and serpentine (?) (Appendix, Table 3, anal. 1). Sample SEB-85-06.
- Fig. 26 – SEM photomicrograph of a merenskyite (MER) inclusion in pyrite (PY) intergrown with pentlandite (PN), all enclosed by silicates. Sample SEB-85-06.
- Fig. 27 – SEM photomicrograph of a chromite grain with typical alteration to magnetite (light) and containing numerous primary, occasionally composite, silicate inclusions. Analyses given in Appendix, Table 3, indicate (a) pargasite (?) analysis 7, (b) pyroxene (?) analysis 8, (c) clinocllore (?) analysis 9, and (d) clinocllore (?) analysis 10 of the matrix silicate. Sample SEB-85-07.





- Fig. 28 – SEM photomicrograph of a merenskyite (MER) (Appendix, Table 6, anal. 2) – pentlandite (PN) – pyrite (PY) composite grain with intergrown serpentine (?) (Appendix, Table 3, anal. 2). Sample SEB-85-07.
- Fig. 29 – SEM photomicrograph of merenskyite (MER) (Appendix, Table 6, anal. 1) – pentlandite (PN) composite grains included in clinochlore (?) (SIL) (Appendix, Table 3, anal. 5). Sample SEB-85-07.
- Fig. 30 – SEM photomicrograph of a large kotulskite (Appendix, Table 3, anal. 3) merenskyite grain (Pd-Te) and numerous smaller kotulskite inclusions (Appendix, Table 3, anal. 4) in violarite (VL) all intergrown with clinochlore (?) (SIL) (Appendix, Table 3, anal. 6). Sample SEB-85-07.
- Fig. 31 – SEM photomicrograph of two sperrylite (SPY) grains (Appendix, Table 7, anal. 4) associated with pyrite (PY) in clinochlore (?) (SIL) (Appendix, Table 3, anal. 3). Sample SEB-85-07.



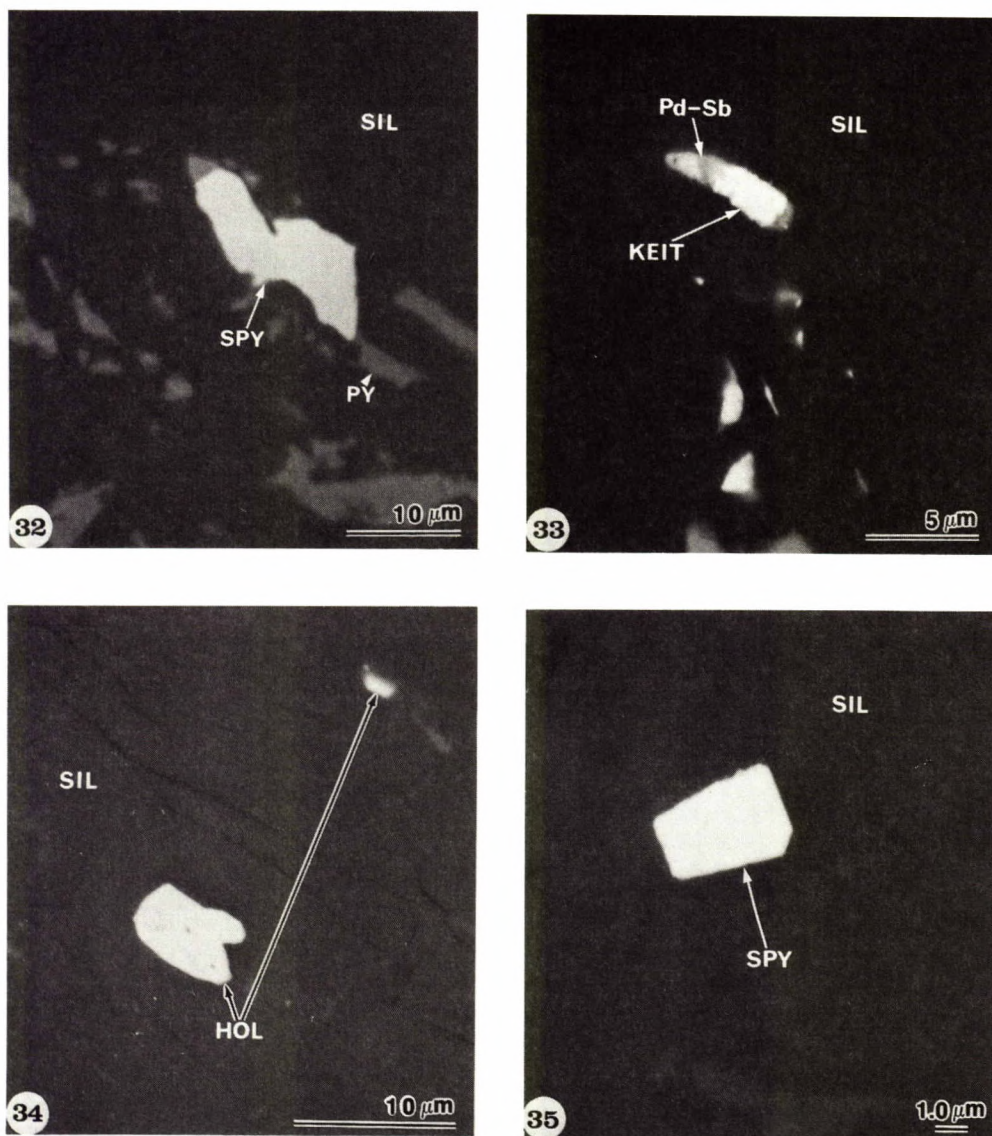


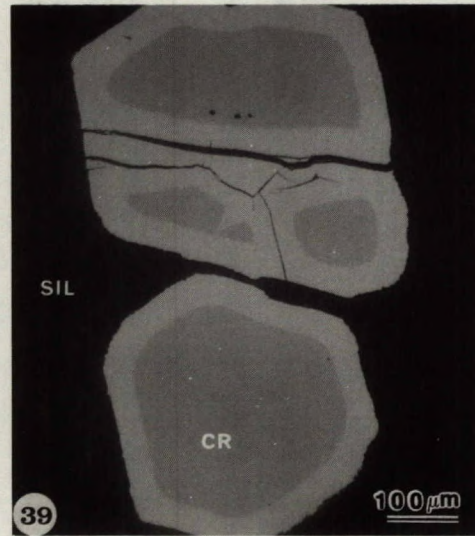
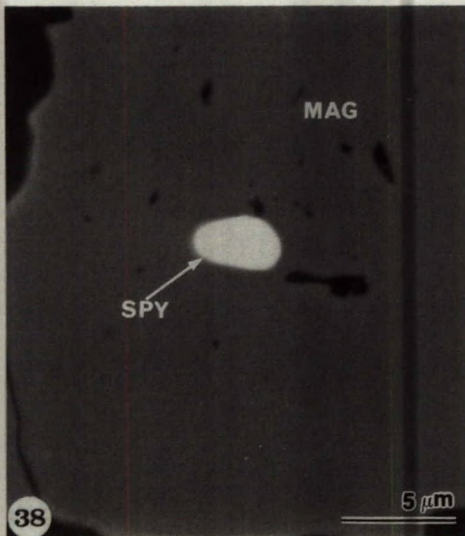
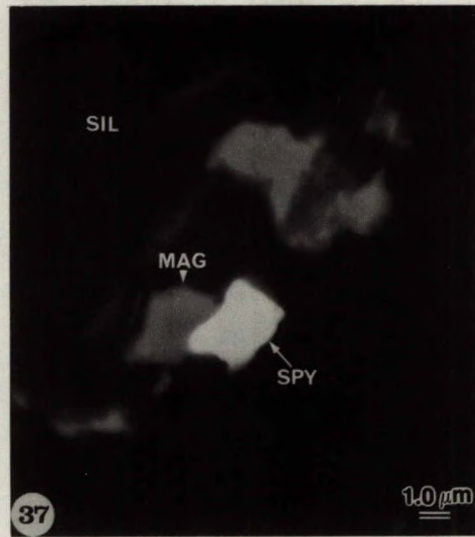
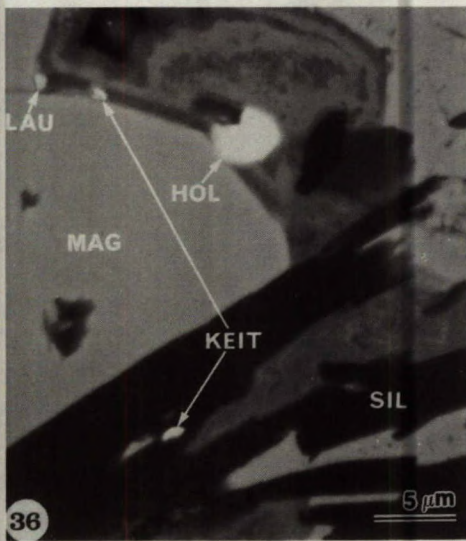
Fig. 32 – SEM photomicrograph of an anhedral sperrylite (SPY) inclusion (Appendix, Table 7, anal. 3) attached to pyrite (PY) in a clinocllore (SIL) matrix (Appendix, Table 3, anal. 4). Sample SEB-85-07.

Fig. 33 – SEM photomicrograph of a keithconnite/mertieite II (?) (KEIT/Pd-Sb) intergrowth with numerous smaller keithconnite inclusions in silicates. Sample SEB-85-10.

Fig. 34 – SEM photomicrograph of two hollingworthite (HOL) inclusions in serpentine (SIL). Sample SEB-85-10.

Fig. 35 – SEM photomicrograph of a euhedral sperrylite (SPY) inclusion in serpentine (SIL). Sample SEB-85-10.





- Fig. 36 – SEM photomicrograph of a large hollingworthite (HOL) grain included in an unidentified Fe silicate and in contact with magnetite (MAG). Small laurite (LAU) and keithconnite (KEIT) inclusions are also included in the Fe silicate at the magnetite contact, and another keithconnite inclusion occurs in serpentine (SIL). Sample SEB-85-10.
- Fig. 37 – SEM photomicrograph of a sperrylite (SPY) inclusion, attached to magnetite (MAG), in a silicate (SIL) matrix. Sample SEB-85-10.
- Fig. 38 – SEM photomicrograph of an elliptical sperrylite (SPY) inclusion in magnetite (MAG). Sample SEB-85-10.
- Fig. 39 – SEM photomicrograph of cumulus chromite (CR) grains with characteristic Fe-rich alteration zones (lighter) in silicate (SIL). Sample SEB-85-16.



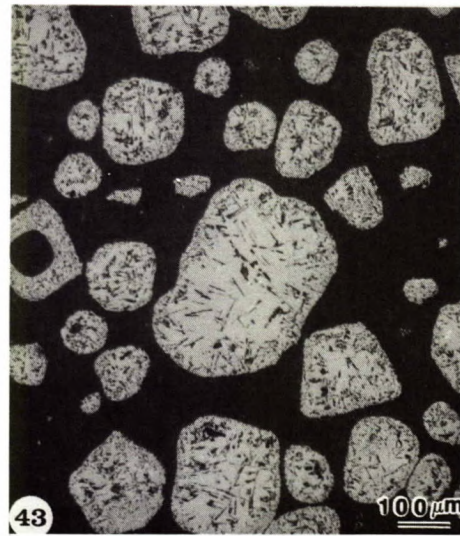
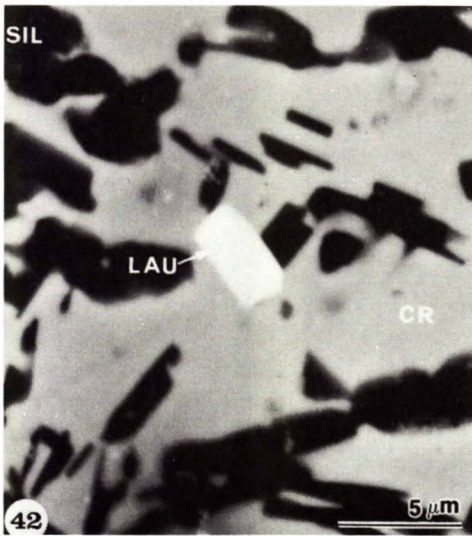
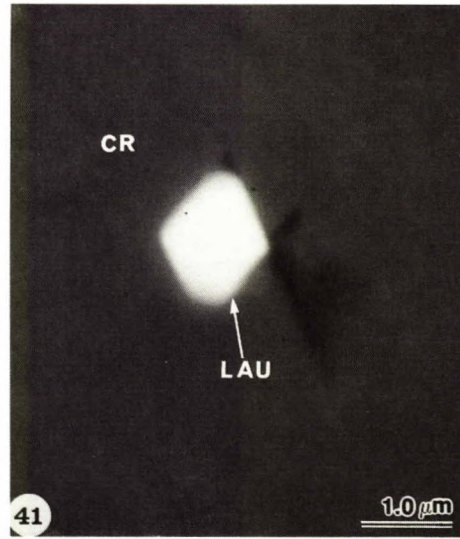
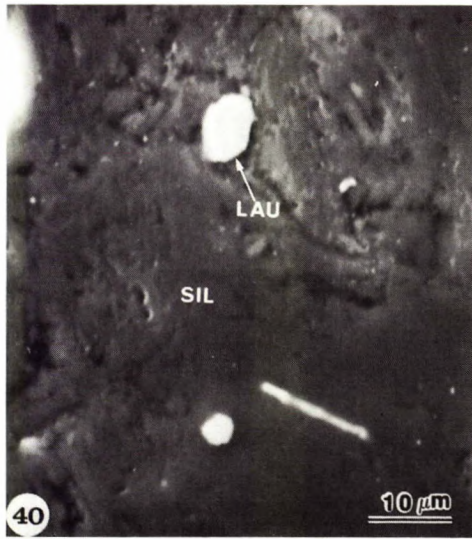


Fig. 40 - SEM photomicrograph of laurite (LAU) inclusions in silicates (SIL). Sample SEB-85-16.

Fig. 41 - SEM photomicrograph of a euhedral laurite (LAU) inclusion in chromite (CR). Sample SEB-85-16.

Fig. 42 - SEM photomicrograph of a euhedral laurite (LAU) inclusion in chromite (CR) intergrown with silicate (SIL). Sample SEB-85-16.

Fig. 43 - SEM photomicrograph of cumulus chromite grains with the "corroded" texture due to fine silicate intergrowths, mostly clinocllore. One chromite grain has a large rounded silicate inclusion as was common for sample SEB-85-07 (Fig. 27). Sample SEB-85-18.



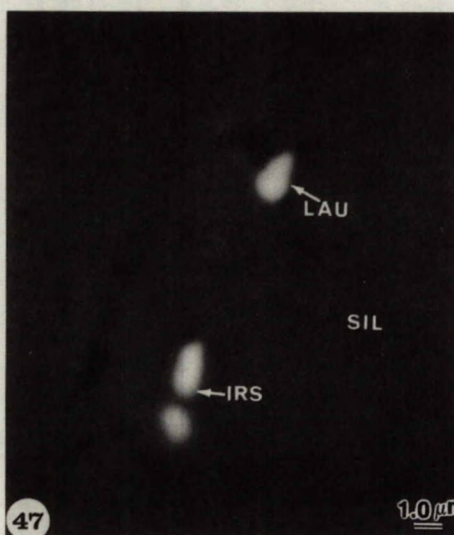
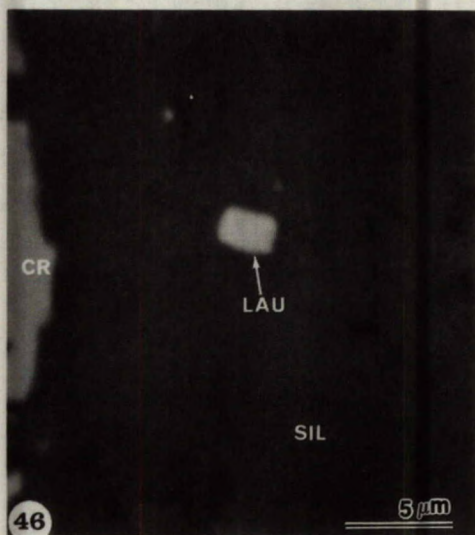
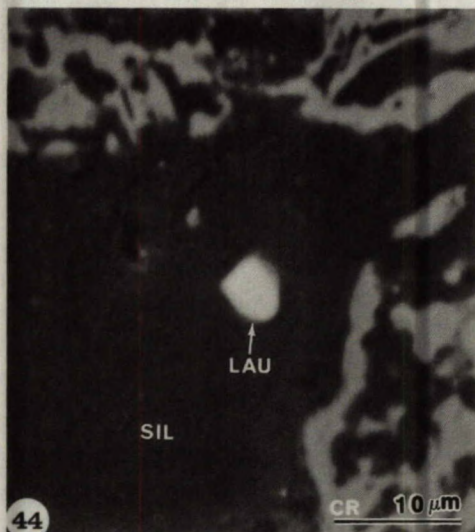


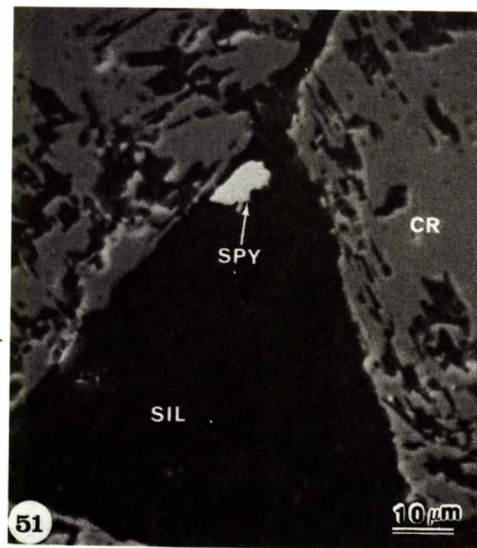
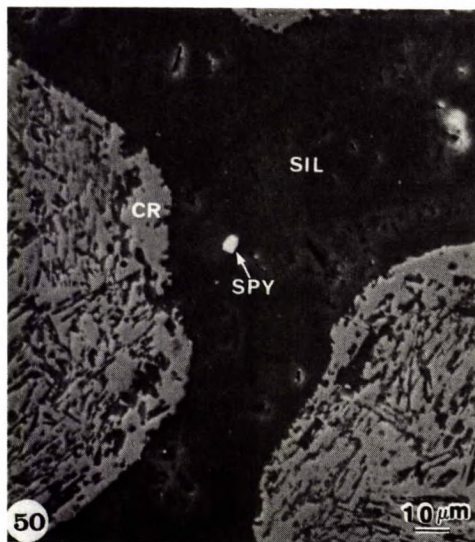
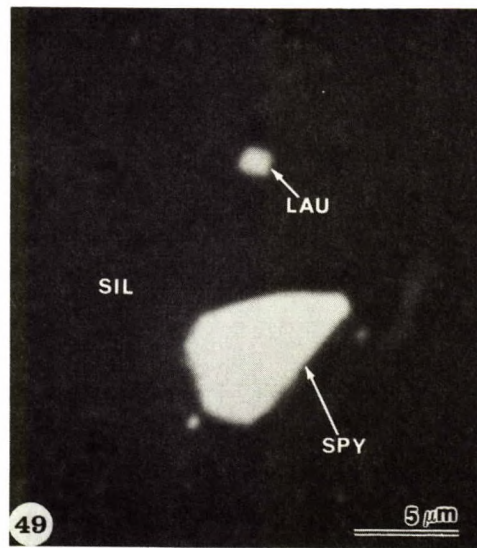
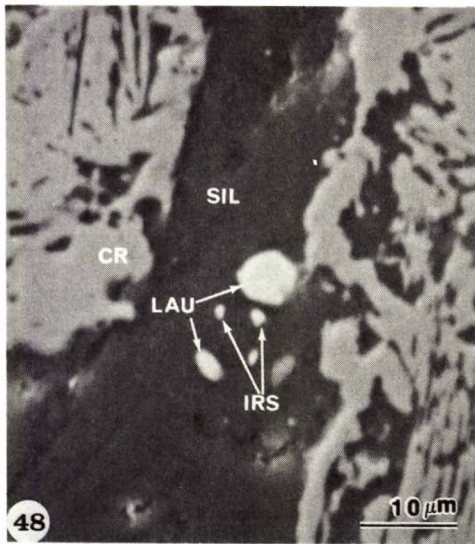
Fig. 44 - SEM photomicrograph of a laurite (LAU) inclusion (Appendix, Table 4, anal. 14) in clinocllore (?) (SIL) next to "corroded" chromite (CR). Sample SEB-85-18.

Fig. 45 - SEM photomicrograph of a laurite (LAU) inclusion in clinocllore (?) (SIL) located between larger chromite (CR) grains. Sample SEB-85-18.

Fig. 46 - Same as Figure 45, but different laurite grain.

Fig. 47 - SEM photomicrograph of a laurite (LAU) and two irarsite (IRS) inclusions in clinocllore (?) (SIL). Sample SEB-85-18.





- Fig. 48 - SEM photomicrograph of laurite (LAU) (Appendix, Table 4, anal. 12) and irarsite (IRS) inclusions in clinocllore (?) (SIL) located between large "corroded" chromite (CR) grains. Sample SEB-85-18.
- Fig. 49 - SEM photomicrograph of inclusions of sperrylite (SPY) and laurite (LAU) in clinocllore (?) (SIL). Sample SEB-85-18.
- Fig. 50 - SEM photomicrograph of a sperrylite (SPY) inclusion in clinocllore (?) (SIL) located between large "corroded" chromite (CR) grains. Sample SEB-85-18.
- Fig. 51 - Same as Figure 50, but different sperrylite grain.



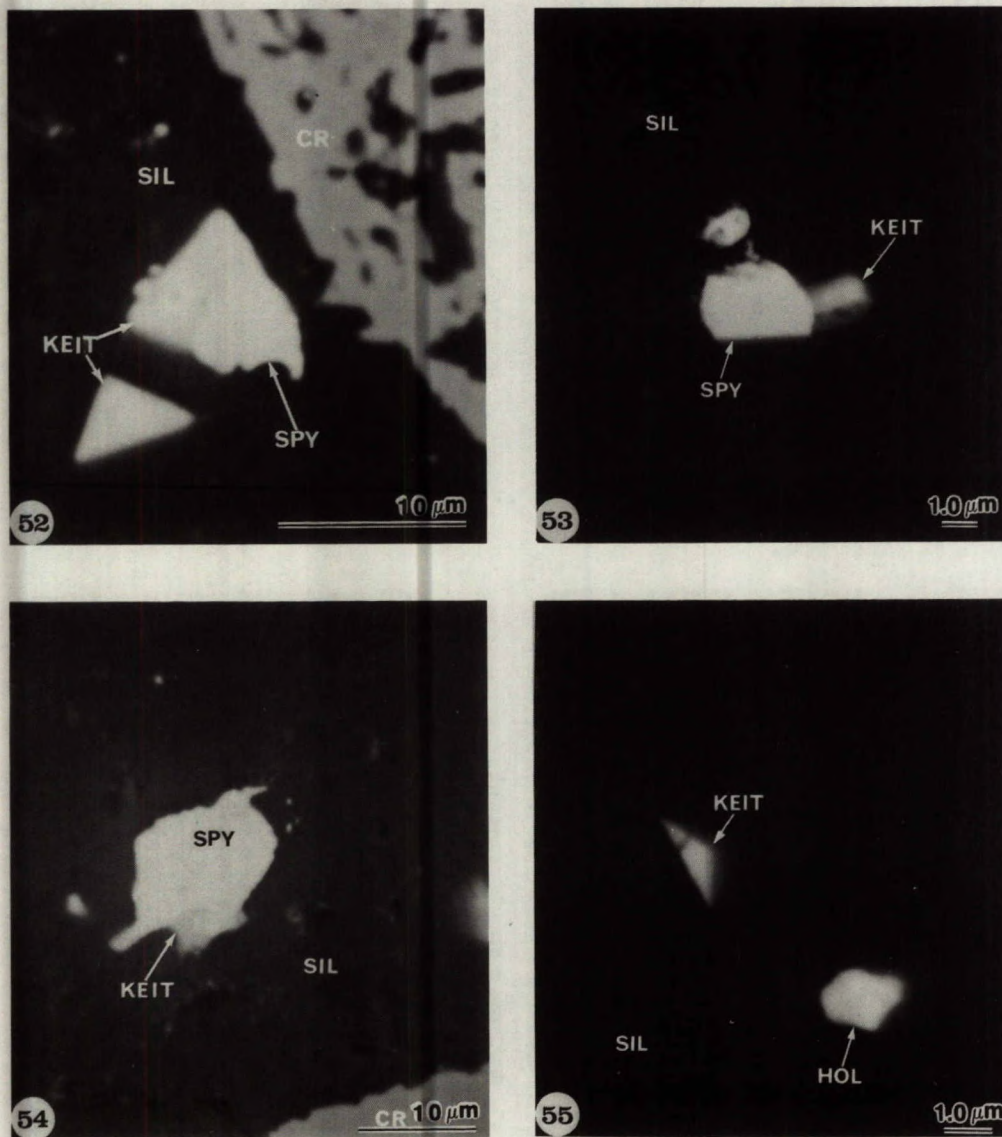


Fig. 52 - SEM photomicrograph of keithconnite (KEIT) grains, one with an attached sperrylite (SPY) grain, included in clinocllore (?) (SIL) close to a large "corroded" chromite (CR) grain. Sample SEB-85-18.

Fig. 53 - SEM photomicrograph of a composite sperrylite (SPY) - keithconnite (KEIT) inclusion in clinocllore (?) (SIL). Sample SEB-85-18.

Fig. 54 - Same as Figure 53, but a different grain with nearby chromite (CR).

Fig. 55 - SEM photomicrograph of inclusions of keithconnite (KEIT) and hollingworthite (HOL) in clinocllore (?) (SIL). Sample SEB-85-18.



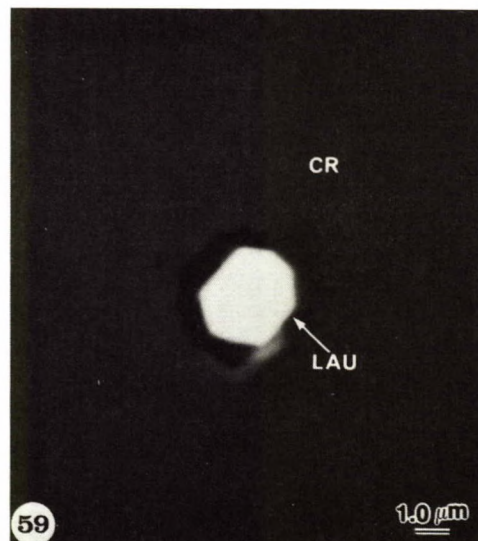
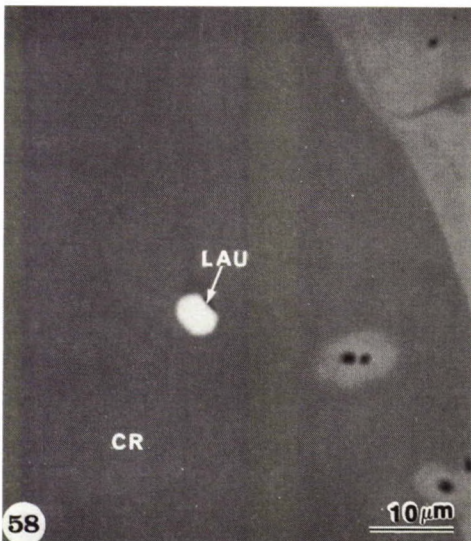
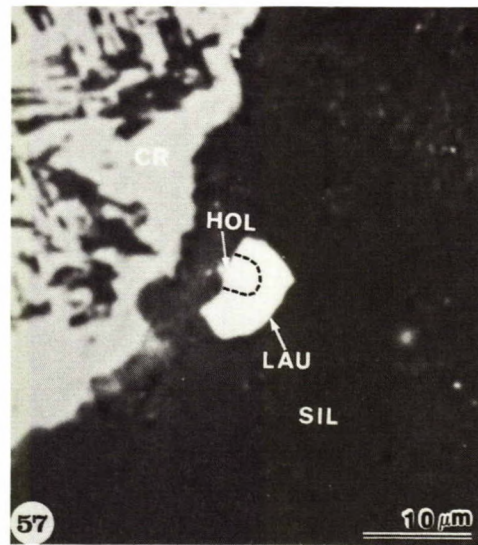
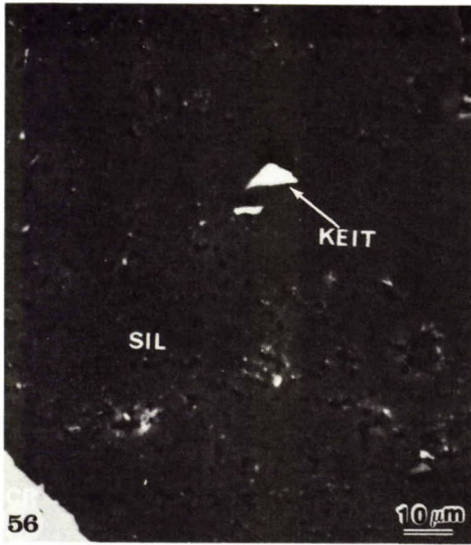


Fig. 56 - SEM photomicrograph of two keithconnite (KEIT) inclusions in clinochlore (?) (SIL) and nearby large "corroded" chromite (CR) grain. Sample SEB-85-18.

Fig. 57 - SEM photomicrograph of a composite laurite (LAU) - hollingworthite (HOL) inclusion in clinochlore (?) (SIL) located near a large "corroded" chromite (CR) grain. Sample SEB-85-18.

Fig. 58 - SEM photomicrograph of a euhedral laurite (LAU) inclusion in chromite (CR) (Appendix, Table 2, anal. 3) with Fe-rich zone (upper right). Sample SEB-85-32.

Fig. 59 - Same as Figure 58, but different laurite grain.



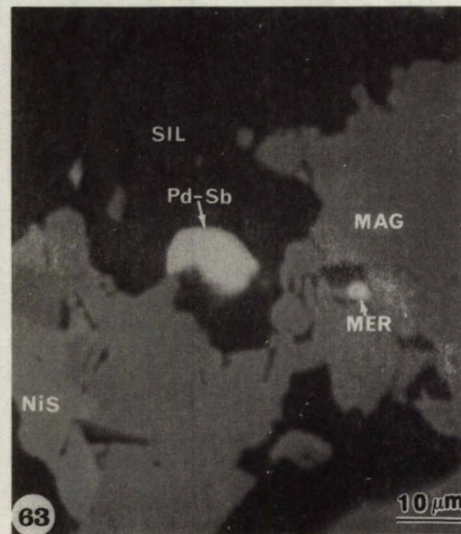
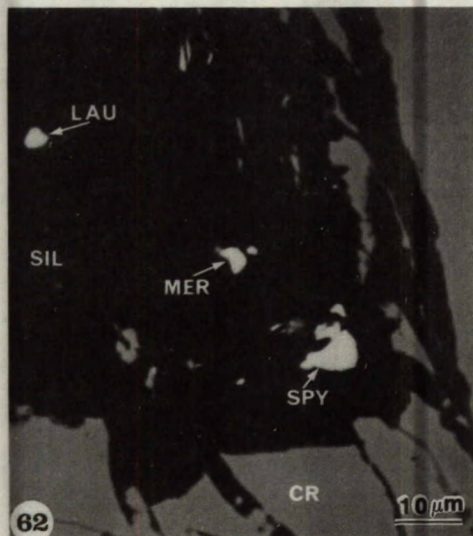
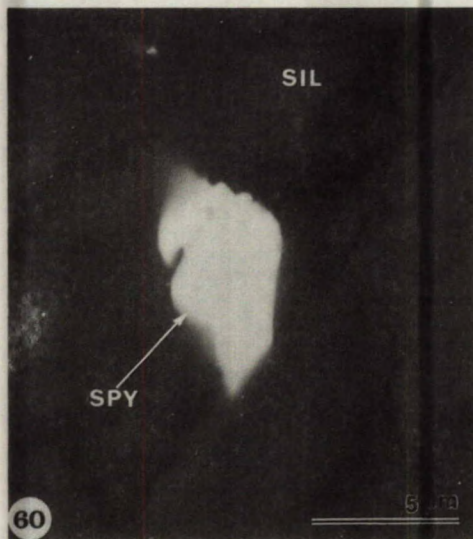


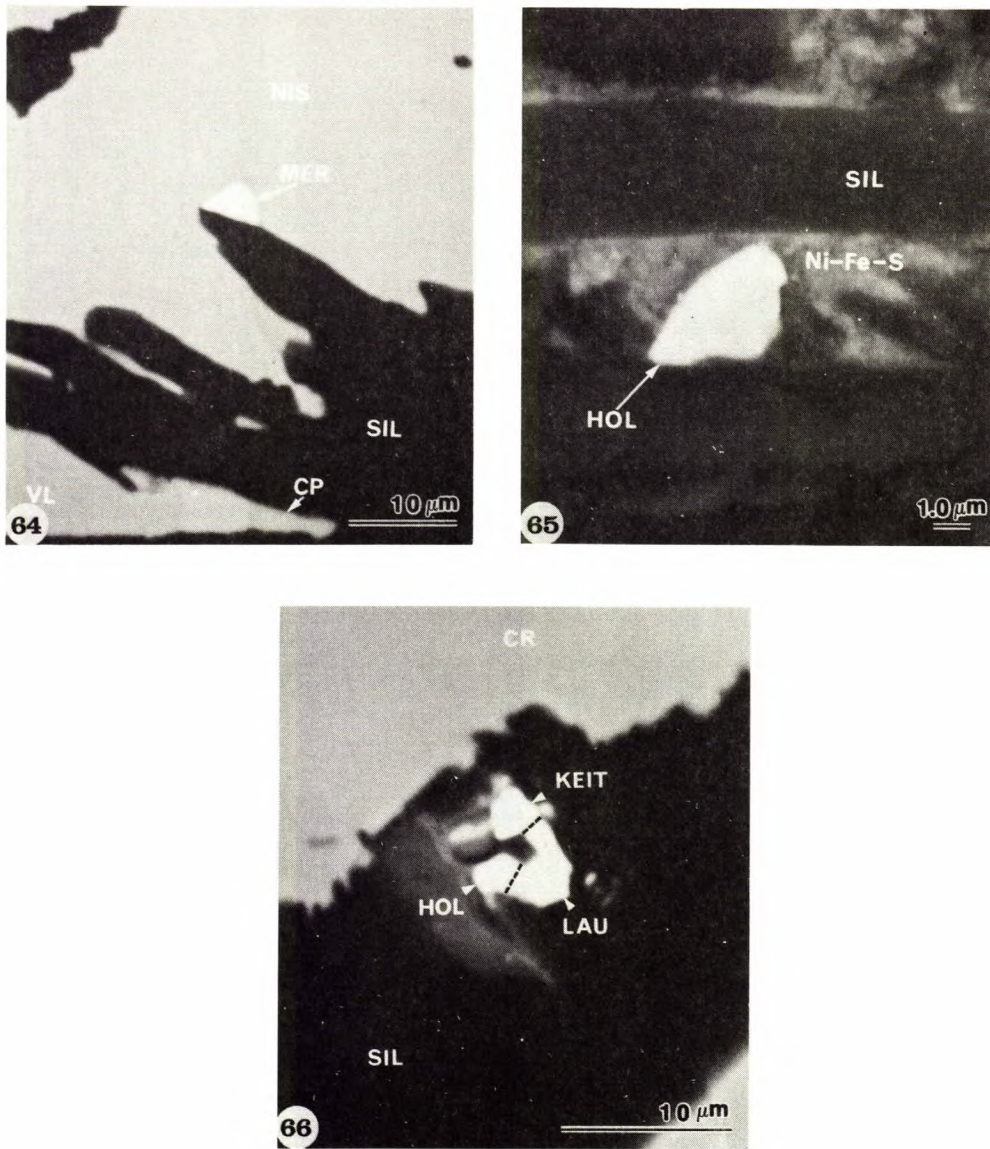
Fig. 60 - SEM photomicrograph of a sperrylite (SPY) grain included in serpentine (Appendix, Table 3, anal. 12). Sample SEB-85-32.

Fig. 61 - SEM photomicrograph of two small sperrylite (SPY) inclusions in serpentine (SIL) (Appendix, Table 3, anal. 20) with a large chromite (CR) grain nearby. Sample SEB-85-32.

Fig. 62 - SEM photomicrograph of several PGM inclusions, sperrylite (SPY), merenskyite (MER), laurite (LAU), in serpentine (SIL) (Appendix, Table 3, anal. 21) and associated large chromite (CR) grains. Sample SEB-85-32.

Fig. 63 - SEM photomicrograph of a mertieite II (Pd-Sb) inclusion (Appendix, Table 6, anal. 7) in pyroxene (?) (SIL) (Appendix, Table 3, anal. 13) and a smaller merenskyite (MER) inclusion in magnetite (MAG) associated with millerite (NiS). Sample SEB-85-32.





- Fig. 64 - SEM photomicrograph of a merenskyite (MER) inclusion in millerite (NiS) in contact with clinocllore (?) (SIL) (Appendix, Table 3, anal. 16). Violarite (VL) and chalcopyrite (CP) are also part of this assemblage. Sample SEB-85-32.
- Fig. 65 - SEM photomicrograph of zoned hollingworthite (HOL) included in a Ni-Fe sulphide grain, itself included in silicates (SIL). Sample SEB-85-32.
- Fig. 66 - SEM photomicrograph of a composite hollingworthite (HOL) - laurite (LAU) - keithconnite (KEIT) inclusion in clinocllore (?) (SIL) (Appendix, Table 3, anal. 19) in close proximity to large chromite (CR) grains. Sample SEB-85-32.

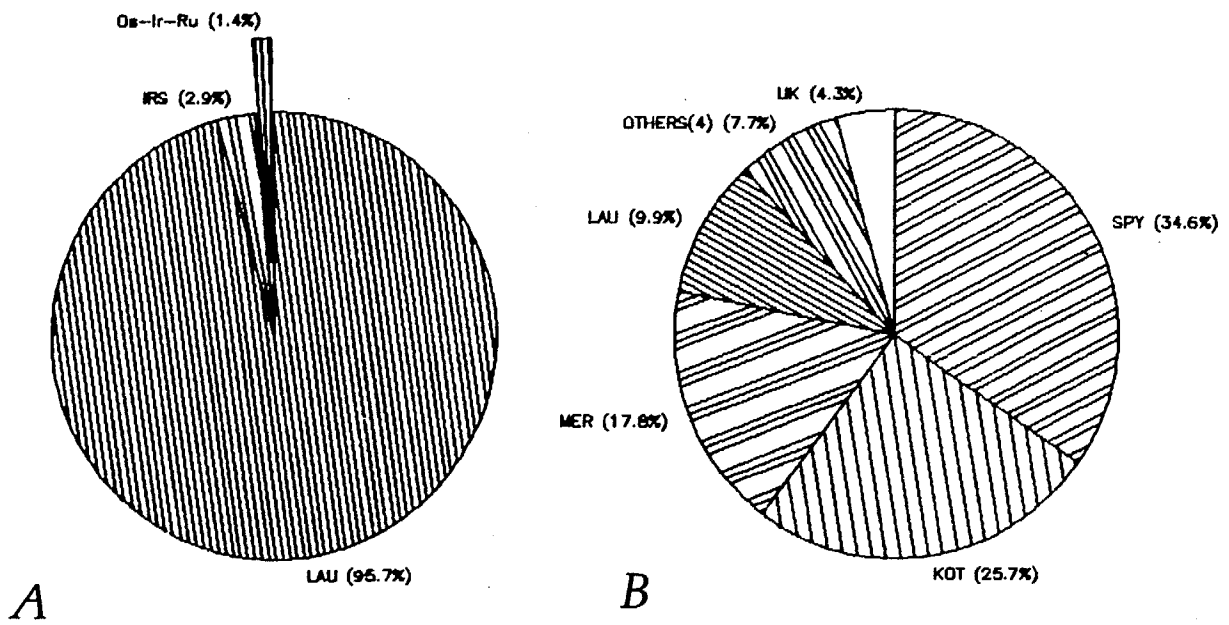


Fig. 67 - Distribution of PGM species, calculated by vol %, in Upper and Lower Main Chromitites (A) and in Lower Group Pt-bearing unit (B). Abbreviations used: LAU = laurite, IRS = irarsite, Os-Ir-Ru = Os-Ir-Ru alloy, SPY = sperrylite, KOT = kotulskite, MER = merenskyite, UK = unidentified minerals.

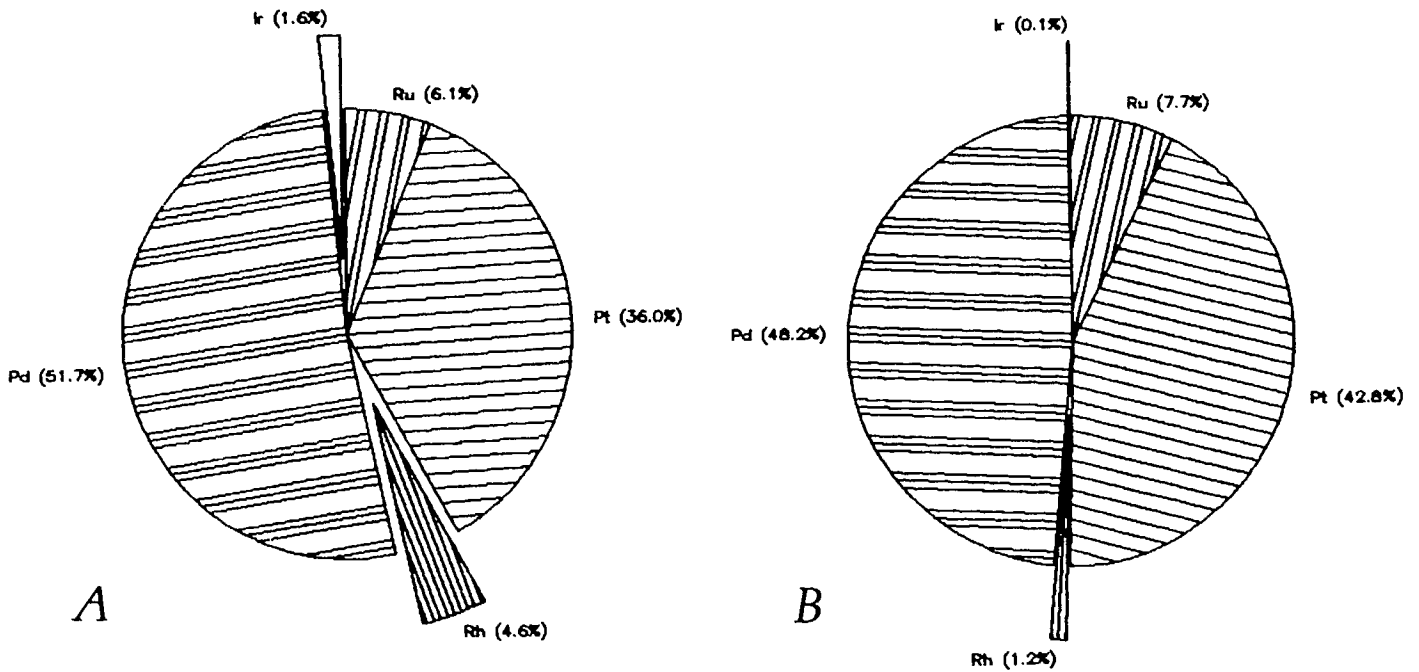


Fig. 68 - Distribution of five PGE for Lower Group Pt-bearing unit from assay data for seven samples (Appendix, Table 2) shown in (A) and as calculated from PGM found (by mass) in (B).

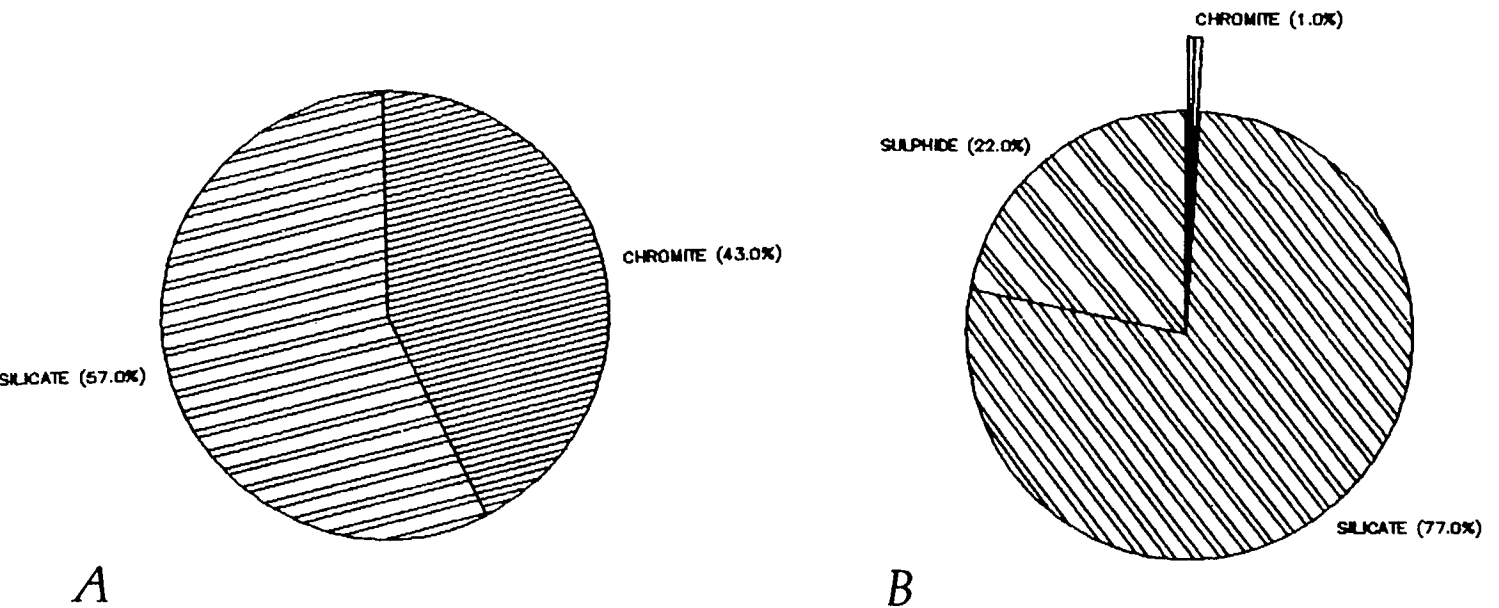


Fig. 69 - Host minerals for PGM inclusions (calculated by vol %) in Upper and Lower Banded Chromitites (A) and in Lower Group Pt-bearing unit (B). Note: chromite host in (B) includes magnetite.

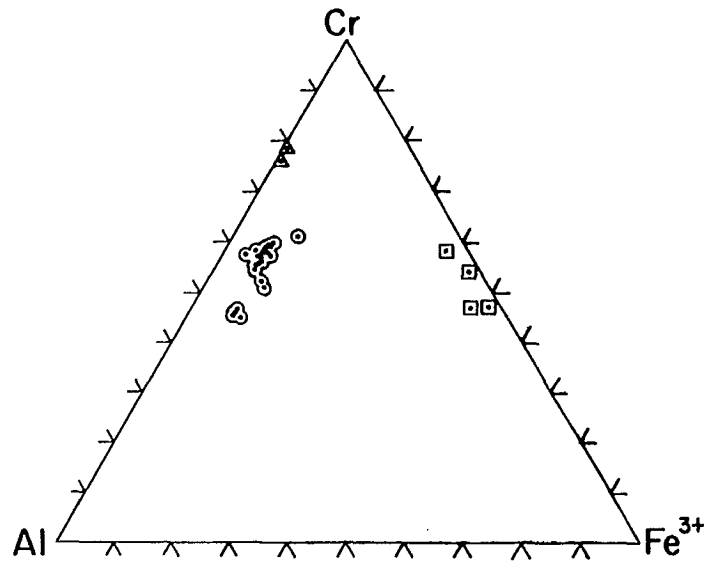


Fig. 70 - Chromite compositions plotted on an Al-Cr-Fe<sup>3+</sup> diagram. Circles are analyses from core areas, squares are from rim areas, and triangles are the Cr-rich (alteration ?) zones.

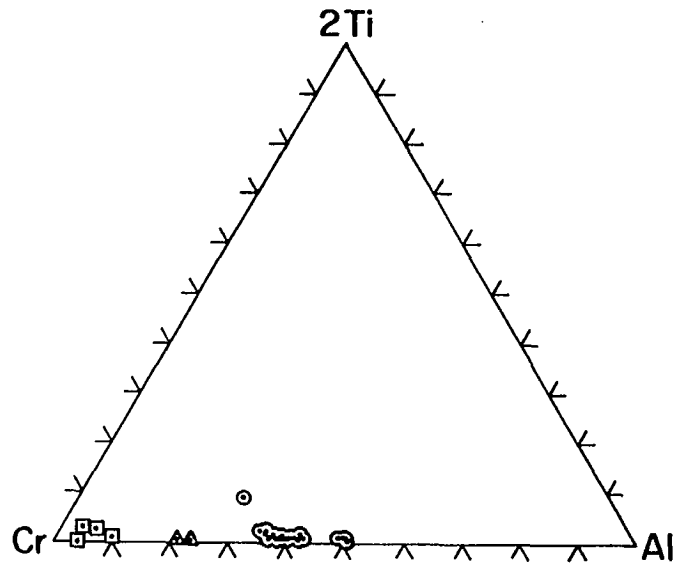


Fig. 71 - Chromite compositions plotted on a Cr-2Ti-Al diagram. Same symbols used as in Figure 70.



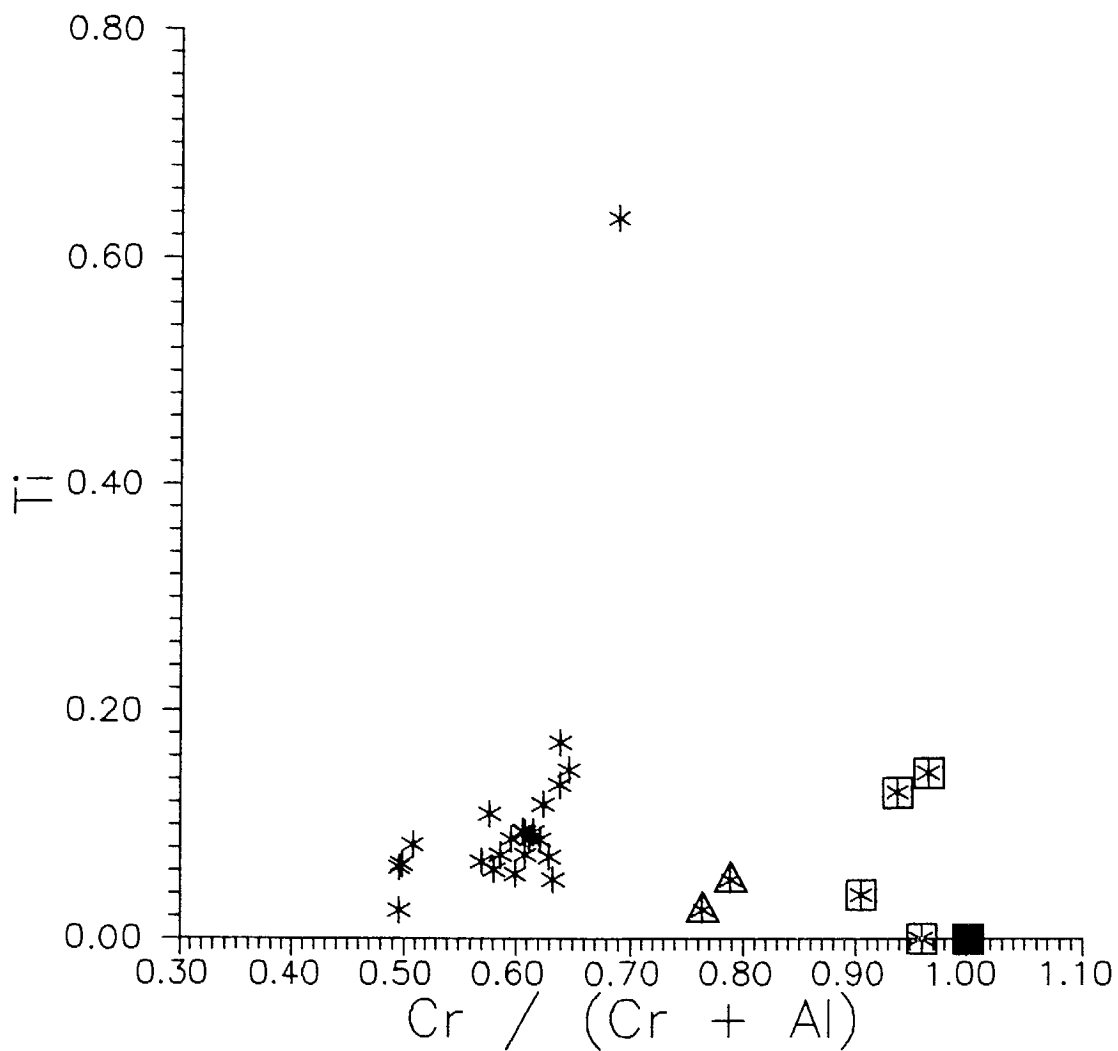


Fig. 72 - A plot of Ti vs Cr/(Cr+Al) for the spinel analyses in Appendix, Table 2. Triangles are for the high Cr analyses (No. 19 and 25), open squares are for rim analyses and the closed square is for the skeletal magnetite intergrowth (No. 3). The single high Ti analysis is from the Lower Group Pt-bearing member.



## **APPENDIX**

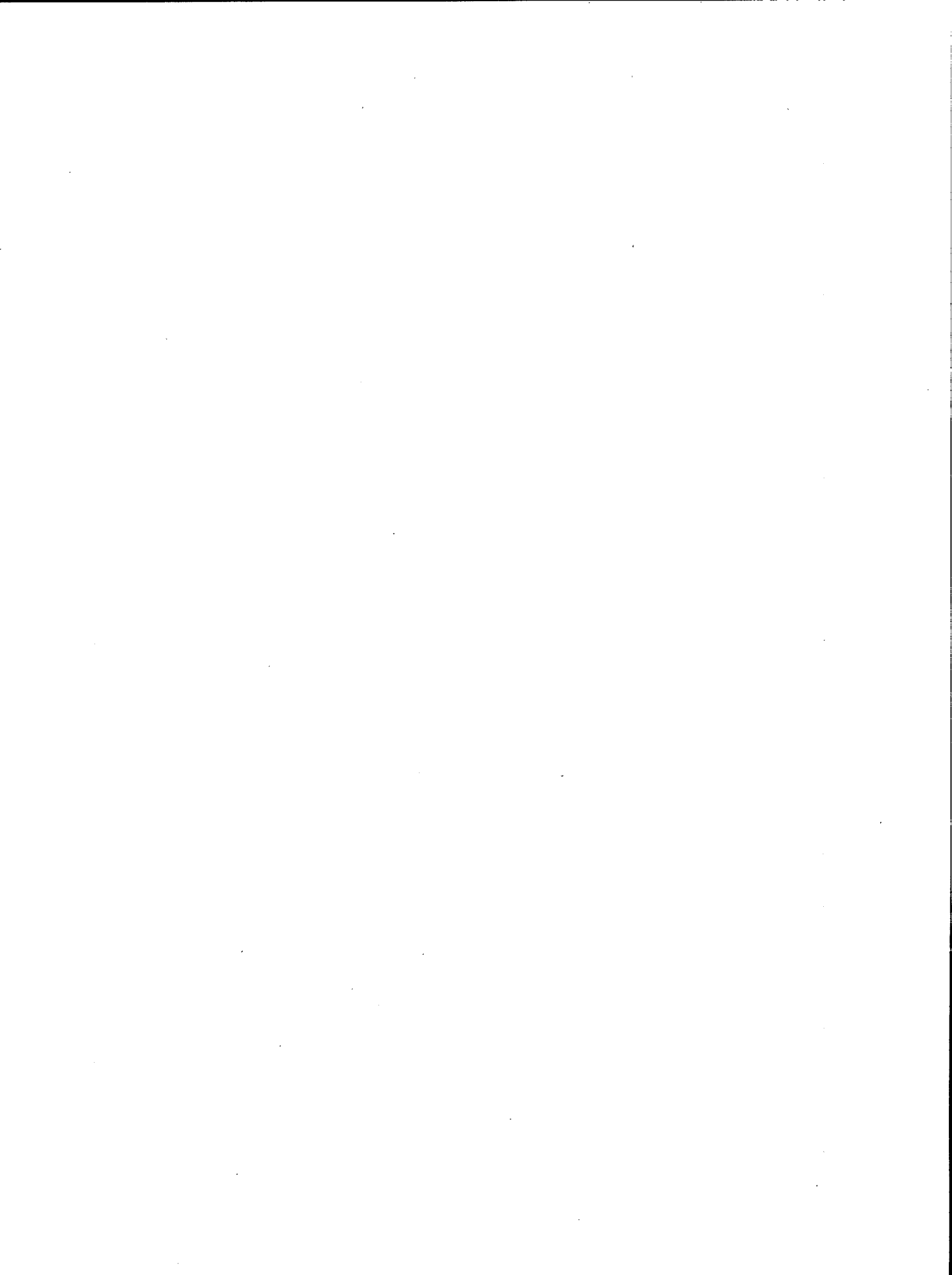


Table 2 - Energy dispersive analyses of spinels from Bird River sill samples

	(1)	(2)	(3)	(4)	(5)	(6)	(7)	(8)
MgO	2.1	0.87	0.28	6.6	0.69	7.6	0.44	4.6
MnO	2.9	3.0	0.12	1.7	2.2	1.4	2.6	1.4
FeO	30.5	28.3	31.0	23.3	29.1	23.0	28.6	27.1
Fe <sub>2</sub> O <sub>3</sub>	7.3	25.7	68.9	7.2	28.4	6.4	35.4	8.3
Cr <sub>2</sub> O <sub>3</sub>	40.2	38.2	0.14	39.0	34.9	36.5	31.3	38.1
TiO <sub>2</sub>	3.0	0.57	0.0	0.55	0.63	0.43	0.0	0.34
SiO <sub>2</sub>	0.37	0.42	0.22	0.25	0.21	0.15	0.28	0.33
Al <sub>2</sub> O <sub>3</sub>	12.2	1.7	0.0	19.2	0.83	23.7	0.89	19.3
Totals	98.57	98.76	100.66	97.80	96.96	99.18	99.51	99.47
NUMBERS OF IONS ON THE BASIS OF 32(O)								
Mg	0.881	0.390	0.127	2.614	0.318	2.897	0.198	1.820
Mn	0.691	0.763	0.031	0.383	0.575	0.303	0.665	0.315
Fe <sup>+2</sup>	7.167	7.102	7.909	5.180	7.318	4.921	7.221	6.021
Fe <sup>+3</sup>	1.537	5.814	15.832	1.442	6.755	1.237	8.038	1.658
Cr	8.941	9.074	0.034	8.193	8.520	7.379	7.476	7.994
Ti	0.635	0.129	0.000	0.110	0.146	0.083	0.000	0.068
Si	0.104	0.126	0.067	0.066	0.065	0.038	0.085	0.088
Al	4.045	0.602	0.000	6.013	0.302	7.142	0.317	6.037
<p>(1) 85-06C, chromite grain (core); (2) 85-06R, same grain (rim); (3) 85-06M, skeletal magnetite intergrowth; (4) 85-07A-C, chromite grain selected at random (core); (5) 85-07A-R, same grain (rim); (6) 85-07B-C, chromite grain shown in Figure 27 (core); (7) 85-07B-R, same grain (rim); (8) 85-32A-9, chromite host of laurite grain (Fig. 58).</p>								

Table 2 - Energy dispersive analyses of spinels from Bird River sill samples (cont'd.../2)

	(9)	(10)	(11)	(12)	(13)	(14)	(15)
MgO	13.2	11.2	8.0	0.36	7.8	8.1	9.0
MnO	0.82	0.60	1.4	1.5	0.64	0.77	0.98
FeO	16.0	19.3	22.6	29.9	22.7	22.9	21.1
Fe <sub>2</sub> O <sub>3</sub>	8.1	6.9	6.7	33.0	5.7	5.7	6.5
Cr <sub>2</sub> O <sub>3</sub>	37.4	37.3	36.0	30.9	45.5	44.8	44.3
TiO <sub>2</sub>	0.35	0.36	0.13	0.17	0.75	0.88	0.61
SiO <sub>2</sub>	0.18	0.29	0.29	0.34	0.0	0.32	0.24
Al <sub>2</sub> O <sub>3</sub>	25.5	25.2	24.6	2.2	16.7	17.0	17.9
Totals	101.55	101.15	99.72	98.37	99.79	100.47	100.63
NUMBERS OF IONS ON THE BASIS OF 32(O)							
Mg	4.726	4.077	3.017	0.163	3.045	3.130	3.438
Mn	0.167	0.124	0.300	0.385	0.142	0.169	0.213
Fe <sup>+2</sup>	3.214	3.936	4.781	7.594	4.961	4.955	4.528
Fe <sup>+3</sup>	1.466	1.272	1.269	7.521	1.128	1.115	1.259
Cr	7.102	7.201	7.200	7.409	9.421	9.182	8.976
Ti	0.063	0.066	0.025	0.039	0.148	0.172	0.118
Si	0.043	0.071	0.073	0.103	0.000	0.083	0.062
Al	7.219	7.253	7.335	0.786	5.155	5.194	5.407
<p>(9) 85-32B-2BC, (10) 85-32-2BC1 and (11) 85-32-2BC2, spot analyses of a typical chromite grain, taken from core to rim, sample SEB-85-32; (12) 85-32-2BR, same grain (rim); (13), (14) and (15) different chromite grains selected at random (EI-86-58).</p>							

Table 2 – Energy dispersive analyses of spinels from Bird River sill samples (cont'd.../3)

	(16)	(17)	(18)	(19)	(20)	(21)	(22)
MgO	8.3	8.6	9.1	6.8	8.3	8.8	9.3
MnO	0.83	0.75	0.56	0.79	0.61	0.78	0.87
FeO	22.1	21.8	21.6	24.3	23.0	21.4	20.4
Fe <sub>2</sub> O <sub>3</sub>	5.2	6.4	5.5	0.35	5.5	5.4	6.3
Cr <sub>2</sub> O <sub>3</sub>	45.6	44.1	43.1	58.4	45.5	46.0	42.3
TiO <sub>2</sub>	0.37	0.61	0.39	0.26	0.70	0.27	0.32
SiO <sub>2</sub>	0.22	0.21	0.20	0.66	0.41	0.26	0.0
Al <sub>2</sub> O <sub>3</sub>	18.0	17.8	20.4	10.5	17.3	17.9	20.5
Totals	100.62	100.27	100.85	102.06	101.32	100.81	99.99
NUMBERS OF IONS ON THE BASIS OF 32(O)							
Mg	3.184	3.309	3.431	2.680	3.175	3.360	3.532
Mn	0.181	0.164	0.120	0.177	0.133	0.169	0.188
Fe <sup>+2</sup>	4.763	4.699	4.574	5.370	4.933	4.590	4.341
Fe <sup>+3</sup>	1.005	1.238	1.052	0.069	1.055	1.044	1.199
Cr	9.278	9.001	8.618	12.207	9.232	9.315	8.522
Ti	0.072	0.118	0.074	0.052	0.135	0.052	0.061
Si	0.057	0.054	0.051	0.174	0.105	0.067	0.000
Al	5.460	5.416	6.081	3.272	5.233	5.404	6.157

(16) 86-58(4) and (17) EI-86-58(5), chromite grains at random; (18) EI-86-58-3, host of a laurite grain (Fig. 5); (19) EI-86-58-3L, same chromite grain, but lighter area (Fig. 5); (20) EI-86-58-5, host of a laurite grain; (21) EI-86-58-8, host of silicate inclusion carrying a laurite grain (Fig. 9); (22) EI-86-58-10, host for Os-Ir-Ru alloy/erlichmanite intergrowth (Fig. 7).

Table 2 - Energy dispersive analyses of spinels from Bird River sill samples (cont'd.../4)

	(23)	(24)	(25)	(26)	(27)	(28)	(29)	(30)	(31)
MgO	10.0	10.0	7.4	9.8	10.0	10.5	10.3	10.5	9.7
MnO	0.80	0.51	0.56	0.66	0.48	0.64	0.45	0.50	1.1
FeO	19.9	20.2	22.6	20.6	20.2	19.5	19.7	19.6	20.7
Fe <sub>2</sub> O <sub>3</sub>	5.4	5.7	0.35	5.7	5.8	5.8	5.1	5.5	4.1
Cr <sub>2</sub> O <sub>3</sub>	43.7	43.7	57.0	44.2	44.1	44.4	45.2	45.7	45.8
TiO <sub>2</sub>	0.46	0.30	0.13	0.46	0.50	0.49	0.39	0.46	0.50
SiO <sub>2</sub>	0.23	0.39	0.29	0.50	0.26	0.33	0.19	0.31	0.45
Al <sub>2</sub> O <sub>3</sub>	19.9	19.6	11.8	18.8	19.2	19.2	19.5	18.7	19.2
Totals	100.39	100.40	100.13	100.72	100.54	100.86	100.83	101.27	101.75

## NUMBERS OF IONS ON THE BASIS OF 32(O)

Mg	3.773	3.775	2.941	3.706	3.778	3.942	3.868	3.934	3.632
Mn	0.172	0.109	0.126	0.142	0.103	0.137	0.096	0.106	0.234
Fe <sup>+2</sup>	4.201	4.271	5.036	4.367	4.280	4.097	4.158	4.124	4.342
Fe <sup>+3</sup>	1.027	1.087	0.070	1.085	1.104	1.106	0.962	1.047	0.805
Cr	8.745	8.750	12.015	8.865	8.837	8.842	9.003	9.082	9.096
Ti	0.088	0.057	0.026	0.088	0.095	0.093	0.074	0.087	0.094
Si	0.058	0.099	0.077	0.127	0.066	0.083	0.048	0.078	0.113
Al	5.937	5.851	3.708	5.621	5.736	5.700	5.791	5.540	5.684

(23) 84-15(1), chromite at random; (24) 84-15(2), chromite at random; (25) 84-15(2R), same chromite grain (rim, lighter grey on BEI); (26) 84-15(3), chromite at random; (27) 84-15-2, chromite host for Os-Ir-Ru alloy grain (Fig. 22); (28) 84-15-7, chromite, host for a laurite grain; (29) 84-15-16, chromite grain, host of a laurite grain (Fig. 18); (30) 84-15-23, chromite grain, host of a laurite inclusion (Fig. 19); (31) 84-15-32, chromite, host of an Os-Ir-Ru alloy inclusion.

These analyses were done on a JEOL microprobe, operated at 15 kV, with a beam current of 12 nanoamperes, using the following X-ray lines and standards: MgK $\alpha$  (MgO); MnK $\alpha$  (MnCO<sub>3</sub>); FeK $\alpha$  and CrK $\alpha$  (metals); TiK $\alpha$  (TiO<sub>2</sub>); SiK $\alpha$  (SiO<sub>2</sub>); AlK $\alpha$  (Al<sub>2</sub>O<sub>3</sub>). Counting times were 100 seconds.



Table 3 – Energy dispersive analyses of silicate minerals from Bird River sill samples

	(1)	(2)	(3)	(4)	(5)	(6)	(7)	(8)	(9)
CaO	0.0	0.0	0.0	0.0	0.0	0.0	11.4	11.8	0.12
Na <sub>2</sub> O	0.0	0.0	0.0	0.0	0.0	0.0	3.4	0.97	0.0
K <sub>2</sub> O	0.0	0.0	0.0	0.0	0.0	0.0	0.0	0.0	0.0
MgO	37.4	37.3	36.2	35.0	34.4	34.5	17.9	23.7	32.5
FeO	4.7	4.6	4.2	3.7	3.7	3.9	0.93	1.6	3.2
Fe <sub>2</sub> O <sub>3</sub>	–	–	–	–	–	–	3.9	–	–
MnO	0.24	0.0	0.22	0.0	0.0	0.23	0.17	0.29	0.32
Cr <sub>2</sub> O <sub>3</sub>	0.0	0.0	0.0	0.10	0.22	3.1	2.5	0.60	3.0
TiO <sub>2</sub>	0.0	0.0	0.0	0.0	0.0	0.12	1.1	0.15	0.2
SiO <sub>2</sub>	42.8	42.1	37.2	35.8	35.3	34.4	45.9	58.4	31.1
Al <sub>2</sub> O <sub>3</sub>	2.8	3.5	9.8	11.8	12.1	11.1	11.8	2.1	17.8
Totals	<u>87.94</u>	<u>87.50</u>	<u>87.62</u>	<u>86.40</u>	<u>85.72</u>	<u>87.35</u>	<u>99.00</u>	<u>99.61</u>	<u>88.25</u>
Ca	–	–	–	–	–	–	1.705	0.441	0.024
Na	–	–	–	–	–	–	0.920	0.066	–
K	–	–	–	–	–	–	–	–	–
Mg	10.377	10.390	10.114	9.881	9.792	9.785	3.725	1.233	9.100
Fe <sup>+2</sup>	0.732	0.719	0.658	0.586	0.591	0.621	0.109	0.047	0.053
Mn	0.038	–	0.035	–	–	0.037	0.020	0.009	0.051
Fe <sup>+3</sup>	–	–	–	–	–	–	0.405	–	–
Cr	–	–	–	0.015	0.033	0.466	0.276	0.017	0.446
Ti	–	–	–	–	–	0.017	0.115	0.004	0.030
Al	–	–	–	–	–	–	0.350	–	–
Si	7.966	7.867	6.972	6.780	6.741	6.545	6.408	2.038	5.842
Al	0.614	0.771	2.165	2.634	2.723	2.489	1.592	0.086	3.941

(1) serpentine? host for sperrylite (Fig. 25); (2) serpentine? host for merenskyite (Fig. 28); (3) clinocllore? host for sperrylite (Fig. 31); (4) clinocllore? host for sperrylite (Fig. 32); (5) 85-07B-4, clinocllore? host for merenskyite (Fig. 29); (6) 85-07B-5, clinocllore? host for kotulskite/merenskyite (Fig. 30); (7) 85-07B-A, chromian magnesio-hastingsitic hornblende, multimineralic inclusion in chromite (Fig. 27); (8) 85-07B-B, augite, same multimineralic inclusion; (9) 85-07B-C, clinocllore? same multimineralic inclusion.

Table 3 – Energy dispersive analyses of silicate minerals from Bird River sill samples (cont'd.../2)

	(10)	(11)	(12)	(13)	(14)	(15)	(16)	(17)
CaO	0.0	0.0	0.0	13.2	0.0	0.0	0.0	0.0
Na <sub>2</sub> O	0.0	0.28	0.0	0.0	0.0	0.0	0.0	0.0
K <sub>2</sub> O	0.0	0.0	0.0	0.0	0.0	0.0	0.0	0.0
MgO	32.6	36.7	36.9	23.4	34.4	32.6	32.7	32.8
FeO	4.2	5.2	5.0	2.5	4.8	4.1	4.4	4.2
MnO	0.0	0.0	0.13	0.0	0.11	0.0	0.0	0.28
Cr <sub>2</sub> O <sub>3</sub>	2.5	0.0	0.0	0.16	1.3	2.0	2.2	2.3
TiO <sub>2</sub>	0.0	0.0	0.0	0.0	0.09	0.20	0.0	0.0
SiO <sub>2</sub>	35.1	42.7	41.4	59.6	36.2	31.0	33.2	32.0
Al <sub>2</sub> O <sub>3</sub>	12.0	3.6	3.8	0.21	12.5	16.1	15.3	15.9
Totals	86.40	88.48	87.23	99.07	89.40	86.00	87.80	87.48
Ca	–	–	–	0.497	–	–	–	–
Na	–	0.101	–	–	–	–	–	–
K	–	–	–	–	–	–	–	–
Mg	9.289	10.138	10.350	1.225	9.473	9.374	9.192	9.283
Fe	0.671	0.806	0.787	0.073	0.742	0.661	0.694	0.667
Mn	–	–	0.021	–	0.017	–	–	0.045
Cr	0.378	–	–	0.004	0.190	0.305	0.328	0.345
Ti	–	–	–	–	0.013	0.029	–	–
Si	6.709	7.913	7.789	2.093	6.688	5.979	6.261	6.075
Al	2.704	0.786	0.843	0.009	2.722	3.660	3.401	3.558

(10) 85-07B-D, clinocllore?, interstitial silicate (Fig. 27); (11) 85-32A-14, serpentine? host for hollingworthite (Fig. 65); (12) 85-32A-13, serpentine? host for sperrylite (Fig. 60); (13) 85-32B-4, augite, host for mertieite II (Fig. 63); (14) 85-32C-1, clinocllore? host of a laurite grain; (15), (16) and (17) clinocllore? spot analyses at random in interstitial gangue, sample SEB-85-32.

Table 3 – Energy dispersive analyses of silicate minerals from Bird River sill samples (cont'd.../3)

	(18)	(19)	(20)	(21)	(22)	(23)	(24)	(25)
CaO	0.0	0.0	0.0	0.0	0.0	0.0	0.0	0.0
Na <sub>2</sub> O	0.0	0.0	0.0	0.0	0.0	0.0	0.0	0.0
K <sub>2</sub> O	0.0	0.0	0.0	0.0	0.0	0.0	0.0	0.0
MgO	32.3	33.4	37.6	36.8	37.0	37.3	33.7	33.5
FeO	4.5	3.8	4.9	4.8	4.5	4.9	4.5	4.6
MnO	0.0	0.12	0.0	0.17	0.0	0.15	0.0	0.25
Cr <sub>2</sub> O <sub>3</sub>	2.5	2.6	0.13	0.0	0.0	0.0	0.14	1.9
TiO <sub>2</sub>	0.23	0.0	0.0	0.0	0.0	0.0	0.0	0.0
SiO <sub>2</sub>	31.3	32.2	41.7	40.9	41.6	42.8	32.6	33.3
Al <sub>2</sub> O <sub>3</sub>	17.3	15.7	4.6	4.1	3.8	3.0	16.3	14.3
Totals	88.13	87.82	88.93	86.77	86.90	88.15	87.24	87.85
Ca	–	–	–	–	–	–	–	–
Na	–	–	–	–	–	–	–	–
K	–	–	–	–	–	–	–	–
Mg	9.084	9.400	10.336	10.374	10.376	10.329	9.492	9.439
Fe	0.710	0.600	0.756	0.759	0.708	0.761	0.711	0.727
Mn	–	0.019	–	0.027	–	0.024	–	0.040
Cr	0.373	0.388	0.019	–	–	–	0.021	0.284
Ti	0.033	–	–	–	–	–	–	–
Si	5.905	6.079	7.690	7.734	7.826	7.951	6.160	6.294
Al	3.847	3.494	1.000	0.914	0.843	0.657	3.630	3.186

(18) and (19) clinocllore? spot analyses at random in interstitial gangue, sample SEB-85-32; (20), (21), (22) and (23) serpentine? spot analyses at random in interstitial gangue, sample SEB-85-32; (24) clinocllore? spot analyses at random in interstitial gangue, sample SEB-85-32; (25) clinocllore? host of keithconnite/laurite/hollingworthite intergrowth (Fig. 66).

Table 3 - Energy dispersive analyses of silicate minerals from Bird River sill samples (cont'd.../4)

	(26)	(27)	(28)	(29)	(30)	(31)	(32)
CaO	0.0	0.0	0.0	0.0	0.0	35.2	0.40
Na <sub>2</sub> O	0.0	0.0	0.0	0.0	0.0	0.0	0.0
K <sub>2</sub> O	0.0	0.0	0.0	0.0	0.0	0.0	0.0
MgO	36.4	35.3	34.2	33.0	33.8	0.44	32.7
FeO	5.1	4.6	1.3	1.1	1.1	0.15	1.4
Fe <sub>2</sub> O <sub>3</sub>	-	-	-	-	-	3.6	-
MnO	0.0	0.0	0.0	0.0	0.10	0.29	0.14
Cr <sub>2</sub> O <sub>3</sub>	0.96	1.3	2.0	1.6	1.4	9.6	2.3
TiO <sub>2</sub>	0.0	0.0	0.0	0.14	0.0	0.50	0.0
SiO <sub>2</sub>	37.4	35.7	31.3	30.8	31.1	38.8	30.1
Al <sub>2</sub> O <sub>3</sub>	10.8	12.4	20.5	19.5	19.7	13.0	20.7
Totals	90.66	89.30	89.30	86.14	87.20	101.58	87.74
Ca	-	-	-	-	-	5.820	0.080
Na	-	-	-	-	-	-	-
K	-	-	-	-	-	-	-
Mg	9.894	9.736	9.313	9.288	9.400	0.101	9.100
Fe <sup>+2</sup>	0.778	0.712	0.199	0.174	0.172	0.019	0.219
Mn	-	-	-	-	0.016	0.038	0.022
Fe <sup>+3</sup>	-	-	-	-	-	0.420	-
Cr	0.138	0.190	0.289	0.239	0.207	1.171	0.339
Ti	-	-	-	0.020	-	0.058	-
Al	-	-	-	-	-	2.351	-
Si	6.819	6.605	5.717	5.815	5.802	5.987	5.619
Al	2.321	2.704	4.414	4.340	4.332	0.013	4.555

(26) 85-32B-6, clinocllore? host for sperrylite grain; (27) 85-32-2B-7, clinocllore? host for sperrylite, merenskyite and laurite grains; (28), (29) and (30) sample EI-86-58, clinocllore? spot analyses at random in interstitial gangue; (31) EI-86-58(4), grossular? selected at random; (32) EI-86-58(5), clinocllore? selected at random in interstitial gangue.

Table 3 – Energy dispersive analyses of silicate minerals from Bird River sill samples (cont'd.../5)

	(33)	(34)	(35)	(36)	(37)	(38)	(39)
CaO	0.0	35.6	35.3	0.0	4.6	24.9	27.7
Na <sub>2</sub> O	0.0	0.0	0.0	0.0	0.15	0.51	0.0
K <sub>2</sub> O	0.0	0.0	0.0	0.0	0.14	0.0	0.0
MgO	33.4	0.84	0.27	32.4	22.5	17.2	0.41
FeO	1.7	0.0	0.72	1.7	3.0	0.85	0.46
Fe <sub>2</sub> O <sub>3</sub>	–	2.2	2.0	–	–	0.50	–
MnO	0.0	0.28	0.18	0.0	0.18	0.0	0.0
Cr <sub>2</sub> O <sub>3</sub>	3.0	7.1	10.8	3.1	1.8	1.4	1.5
TiO <sub>2</sub>	0.0	1.1	1.1	0.0	0.0	0.15	35.8
SiO <sub>2</sub>	30.8	38.5	38.8	30.3	39.0	54.9	30.9
Al <sub>2</sub> O <sub>3</sub>	20.8	15.1	13.3	20.3	2.4	2.5	2.0
Totals	89.70	100.72	102.47	87.80	73.77	102.91	98.77
Ca	–	5.872	5.790	–	1.098	0.941	3.915
Na	–	–	–	–	0.065	0.035	–
K	–	–	–	–	0.040	–	–
Mg	9.103	0.193	0.062	9.022	7.469	0.904	0.081
Fe <sup>+2</sup>	0.260	–	0.092	0.266	0.559	0.024	0.051
Mn	–	0.037	0.023	–	0.034	–	–
Fe <sup>+3</sup>	–	0.257	0.228	–	–	0.013	–
Cr	0.434	0.864	1.307	0.458	0.317	0.039	0.156
Ti	–	0.127	0.127	–	–	0.004	3.551
Al	–	2.666	2.339	–	–	0.039	–
Si	5.631	5.926	5.939	5.660	8.684	1.935	4.075
Al	4.483	0.074	0.061	4.470	0.630	0.065	0.311

(33) EI-86-58-9, clinocllore? host of laurite grain (Fig. 8); (34) EI-86-58-9G, grossular? same area (Fig. 8); (35) EI-86-58-6, grossular, selected at random; (36) EI-86-58(7), clinocllore? part of a multiminerale silicate intergrowth in chromite (Fig. 10); (37) EI-86-58(8), (mixture?) same multiminerale silicate grain in chromite; (38) EI-86-58(9), Cr-diopside, same multiminerale silicate grain; (39) EI-86-58(10), sphene, also from that multiminerale grain.

Table 3 - Energy dispersive analyses of silicate minerals from Bird River sill samples (cont'd.../6)

	(40)	(41)	(42)	(43)	(44)	(45)	(46)
CaO	0.0	0.0	0.0	35.8	37.2	0.10	36.8
Na <sub>2</sub> O	0.21	0.0	0.31	0.0	0.0	0.0	0.0
K <sub>2</sub> O	0.0	0.0	0.0	0.0	0.0	0.0	0.0
MgO	31.3	33.1	34.0	0.41	0.0	35.7	0.0
FeO	1.6	1.2	0.83	0.0	0.43	0.96	0.0
Fe <sub>2</sub> O <sub>3</sub>	-	-	-	2.7	0.97	-	2.2
MnO	0.0	0.09	0.12	0.0	0.0	0.0	0.13
Cr <sub>2</sub> O <sub>3</sub>	4.2	0.95	1.0	7.0	4.7	0.82	5.4
TiO <sub>2</sub>	0.0	0.0	0.0	0.34	0.11	0.0	0.23
SiO <sub>2</sub>	29.4	31.3	32.6	39.1	39.8	34.0	39.8
Al <sub>2</sub> O <sub>3</sub>	19.6	20.7	19.2	15.5	19.1	17.1	17.0
Totals	86.31	87.34	88.06	100.85	102.31	88.68	101.56
Ca	-	-	-	5.886	5.963	0.020	5.972
Na	0.078	-	0.111	-	-	-	-
K	-	-	-	-	-	-	-
Mg	8.909	9.165	9.330	0.094	-	9.718	-
Fe <sup>+2</sup>	0.256	0.186	0.128	-	0.053	0.147	-
Mn	-	0.014	0.019	-	-	-	0.017
Fe <sup>+3</sup>	-	-	-	0.308	0.109	-	0.253
Cr	0.634	0.140	0.146	0.849	0.556	0.118	0.647
Ti	-	-	-	0.039	0.012	-	0.026
Al	-	-	-	2.804	3.322	-	3.035
Si	5.614	5.814	6.001	6.000	5.954	6.209	6.028
Al	4.411	4.532	4.166	0.000	0.046	3.681	0.000

(40) EI-86-58-8, clinocllore? host of laurite grain and enclosed in chromite (Fig. 9); (41) 84-15(1) and (42) 84-15(2), clinocllore? selected at random; (43) 84-15(3) and (44) 84-15(4), grossular? selected at random in the interstitial gangue material; (45) 84-15(5), clinocllore? at random in interstitial gangue; (46) 84-15-17G, grossular? host of laurite inclusions.

Table 3 – Energy dispersive analyses of silicate minerals from Bird River sill samples (cont'd.../7)

	(47)	(48)	(49)	(50)	(51)	(52)	(53)
CaO	0.10	34.8	0.0	0.0	0.24	37.4	0.0
Na <sub>2</sub> O	0.0	0.0	0.15	0.0	0.0	0.0	0.0
K <sub>2</sub> O	0.0	0.0	0.0	0.0	0.0	0.0	0.0
MgO	36.0	1.7	35.1	31.4	33.5	0.0	33.6
FeO	1.2	0.07	1.5	1.5	1.1	0.11	1.2
Fe <sub>2</sub> O <sub>3</sub>	–	1.9	–	–	–	2.0	–
MnO	0.0	0.0	0.0	0.0	0.0	0.0	0.0
Cr <sub>2</sub> O <sub>3</sub>	0.89	5.8	1.4	1.9	1.2	4.7	0.82
TiO <sub>2</sub>	0.0	0.37	0.0	0.0	0.0	0.40	0.0
SiO <sub>2</sub>	34.7	38.9	31.6	27.3	30.7	40.1	31.0
Al <sub>2</sub> O <sub>3</sub>	15.7	17.7	20.1	25.7	20.2	18.2	20.3
Totals	88.59	101.24	89.85	87.80	86.94	102.91	86.92
Ca	0.020	5.643	–	–	0.048	5.975	–
Na	–	–	0.053	–	–	–	–
K	–	–	–	–	–	–	–
Mg	9.822	0.384	9.506	8.717	9.343	–	9.352
Fe <sup>+2</sup>	0.184	0.009	0.228	0.234	0.172	0.013	0.187
Mn	–	–	–	–	–	–	–
Fe <sup>+3</sup>	–	0.219	–	–	–	0.224	–
Cr	0.129	0.694	0.201	0.280	0.178	0.554	0.121
Ti	–	0.042	–	–	–	0.045	–
Al	–	3.045	–	–	–	3.177	–
Si	6.351	5.887	5.741	5.084	5.744	5.979	5.788
Al	3.387	0.113	4.304	5.641	4.455	0.021	4.468

(47) 84-15-17C, clinocllore? accessory mineral with grossular which hosts laurite grains; (48) 84-15-24G, grossular host of a laurite grain (Fig. 16); (49) 84-15-24C, clinocllore? accessory mineral with grossular which hosts a laurite grain (Fig. 16); (50) 84-15-26, clinocllore? host of irarsite and laurite grains (Fig. 14); (51) 84-15-35C, clinocllore? host for laurite and unknown (Pd,Pt,Ru)-(S,As,Sb) (Fig. 15); (52) 84-15-35G, grossular? accessory mineral to clinocllore that carries laurite grain (Fig. 15); (53) 84-15-36, clinocllore? host for a laurite grain (Fig. 13). These analyses were done on a JEOL-733 electron microprobe, operated at 15 kV, with a beam current of 12 nanoamperes, using the following X-ray lines and standards: CaK $\alpha$  (apatite); NaK $\alpha$  (NaCl); KK $\alpha$  (orthoclase); MgK $\alpha$  (MgO); FeK $\alpha$ , CrK $\alpha$  (metals); MnK $\alpha$  (MnCO<sub>3</sub>); TiK $\alpha$  (TiO<sub>2</sub>); SiK $\alpha$  (SiO<sub>2</sub>); AlK $\alpha$  (Al<sub>2</sub>O<sub>3</sub>). Counting time was 100 seconds. Calculations of the numbers of ions were done on the basis of 28 oxygen equivalents for the clinocllores, 24 oxygens for the garnets, and 6 oxygens for the amphiboles and pyroxenes.

Table 4 - Electron microprobe analyses of laurite from Bird River sill samples

Analysis no.	Weight per cent											Atomic proportions											
	Ru	Os	Rh	Pd	Ir	Pt	Fe	Ni	S	As	Totals	Ru	Os	Rh	Pd	Ir	Pt	Fe	Ni	Σ	S	As	Σ
1.	51.9	5.1	0.45	0.49	3.3	0.11	-	n.d.	37.6	0.19	99.14	0.88	0.05	0.01	0.01	0.03	<0.01	-	-	0.98	2.02	<0.01	2.02
2.	52.5	4.9	0.46	0.39	2.8	n.d.	-	n.d.	37.7	0.17	98.92	0.89	0.04	0.01	0.01	0.03	-	-	-	0.98	2.02	<0.01	2.02
3.	49.4	2.8	0.44	0.35	3.4	n.d.	3.6	0.43	39.4	0.20	100.02	0.80	0.02	0.01	0.01	0.03	-	0.11	0.01	0.98	2.01	0.01	2.02
4.	54.0	3.4	0.49	0.38	2.9	0.24	0.15	0.10	38.2	0.16	100.02	0.90	0.03	0.01	0.01	0.03	0.01	<0.01	<0.01	0.98	2.01	<0.01	2.01
5.	55.4	3.0	0.39	0.44	2.5	0.17	-	n.d.	38.4	0.18	100.48	0.92	0.03	0.01	0.01	0.02	<0.01	-	-	0.99	2.01	<0.01	2.01
6.	55.3	2.1	0.34	0.38	2.1	n.d.	-	n.d.	38.4	0.12	98.74	0.92	0.02	0.01	0.01	0.02	-	-	-	0.98	2.02	<0.01	2.02
7.	57.7	0.12	1.6	0.15	n.d.	n.d.	0.46	0.16	39.2	0.74	100*	0.94	<0.01	0.02	<0.01	-	-	0.01	<0.01	0.98	2.00	0.02	2.02
8.	57.4	0.36	1.5	0.38	0.22	0.20	-	0.15	38.2	0.69	99.10	0.95	<0.01	0.02	0.01	<0.01	<0.01	-	<0.01	0.99	1.99	0.02	2.01
9.	56.1	1.4	1.5	0.32	n.d.	0.22	-	0.12	38.4	0.50	98.56	0.93	0.01	0.02	0.01	-	<0.01	-	<0.01	0.98	2.01	0.01	2.02
10.	39.7	15.4	0.65	0.36	7.5	0.11	0.34	0.13	35.8	n.d.	100*	0.72	0.15	0.01	0.01	0.07	<0.01	0.01	<0.01	0.97	2.03	-	2.03
11.	42.8	4.9	3.7	0.30	n.d.	1.9	3.9	0.54	35.7	6.3	100*	0.72	0.04	0.06	<0.01	-	0.02	0.12	0.02	0.98	1.88	0.14	2.02
12.	42.9	15.7	0.16	0.43	1.2	0.29	1.7	0.31	35.7	1.6	100*	0.75	0.15	<0.01	0.01	0.01	<0.01	0.05	0.01	0.98	1.98	0.04	2.02
13.	23.6	29.8	5.6	0.63	0.60	3.8	1.2	0.19	26.8	7.7	100*	0.49	0.33	0.11	0.01	0.01	0.04	0.04	0.01	1.04	1.75	0.21	1.96
14.	38.5	23.3	0.59	0.56	1.2	n.d.	1.2	0.10	33.5	1.1	100*	0.71	0.23	0.01	0.01	0.01	-	0.04	<0.01	1.01	1.96	0.03	1.99

\* Recalculated to 100%; Sb sought, but not detected. The analyses were done by wavelength spectrometry on a JEOL-733 electron microprobe, operated at 15 kV, with a beam current of 25 nanoamperes, using the following X-ray lines and standards: RuL $\alpha$ , OsL $\alpha$ , PdL $\alpha$ , IrL $\alpha$ , PtL $\alpha$ , FeK $\alpha$ , NiK $\alpha$  (metals); AsL $\alpha$  (InAs); SK $\alpha$  (pyrite). Some of the analyses with low totals were normalized to 100%. Low totals may have been obtained by a combination of small size and geometry of the grains. Corrections were applied for interferences of RuL $\beta_2$  and RhL $\beta_1$  on PdL $\alpha$  and RuL $\beta_1$  on RhL $\alpha_1$ .

1. area 3, sample EI-86-58, 4x6  $\mu$ m, in chromite (Fig. 5, Table 2).
2. area 5, sample EI-86-58, 4x7  $\mu$ m, in chromite (Fig. 6, Table 2).
3. area 9, sample EI-86-58, 5x14  $\mu$ m, in clinocllore(?) (Fig. 8, Table 5).
4. area 8, sample EI-86-58, 4x4  $\mu$ m, in clinocllore(?) but enclosed in chromite (Fig. 9, Tables 2 and 3).
5. area 16, sample 84-15, 5x6  $\mu$ m, in chromite (Fig. 18, Table 2).
6. area 23, sample 84-15, 4x10  $\mu$ m, in chromite (Fig. 19, Table 2).
7. area 24, sample 84-15, 2x3  $\mu$ m, in clinocllore(?) (Fig. 16, Table 3).
8. area 26, sample 84-15, 5x5  $\mu$ m, in clinocllore(?) (Fig. 14, Table 3).
9. area 26, sample 84-15, 5x5  $\mu$ m, in clinocllore(?) (Fig. 14, Table 3).
10. area 9, sample 85-32A, 3x5  $\mu$ m, in chromite (Fig. 58, Table 2).
11. area 1, sample 85-32C, 7x12  $\mu$ m, in clinocllore(?) (Table 3).
12. area 26, sample 85-18, 6x6  $\mu$ m, in clinocllore(?) (Fig. 48).
13. area 10A, sample 85-18, 6x9  $\mu$ m, in clinocllore(?) intergrown with laurite.
14. area 10B, sample 85-18, 3x5  $\mu$ m, in clinocllore(?) (Fig. 44).



Table 5 – Electron microprobe analyses of pentlandite from Bird River sill (sample SEB-84-7)

Spot no.	Weight per cent					Atomic proportions				
	Fe	Ni	Co	S	Totals	Fe	Ni	Co	Σ	S
1	23.7	42.3	1.1	32.7	99.8	3.30	5.61	0.15	9.06	7.94
2	24.3	42.3	1.1	33.0	100.7	3.36	5.56	0.14	9.06	7.94
3	23.2	42.8	1.1	32.8	99.9	3.23	5.67	0.14	9.04	7.96
4	23.2	42.5	1.1	32.3	99.1	3.26	5.68	0.15	9.09	7.91
5	23.2	42.9	0.77	32.6	99.47	3.25	5.71	0.10	9.06	7.94
6	24.4	41.9	0.40	32.1	98.80	3.44	5.62	0.05	9.11	7.88
7	24.7	41.9	0.31	32.9	99.81	3.44	5.55	0.04	9.03	7.97
8	24.1	42.5	0.32	32.4	99.32	3.38	5.67	0.04	9.09	7.91
9	24.5	42.1	0.31	32.5	99.41	3.43	5.61	0.04	9.08	7.92
10	24.4	42.5	0.59	32.5	99.99	3.40	5.63	0.08	9.11	7.89
11	24.3	42.4	0.60	32.7	100.00	3.38	5.61	0.08	9.07	7.93
12	24.8	42.0	0.62	32.7	100.12	3.45	5.55	0.08	9.08	7.92
Average	24.1	42.3	0.69	32.6	99.69	3.36	5.62	0.09	9.07	7.93

The analyses are of six grains from the polished thin section, by WDS at 20 kV, with a beam current of 20 nanoamperes, using the following X-ray lines and standards: FeK $\alpha$ , NiK $\alpha$ , SK $\alpha$  (synthetic Fe<sub>4.0</sub>Ni<sub>5.0</sub>S<sub>7.99</sub>Se<sub>0.01</sub>); CoK $\alpha$  (metal). Pd was not detected at a minimum detection limit of 0.036 wt %.

Table 6 – Electron microprobe analyses of Pd minerals from Bird River sill samples

Sample no.	Weight per cent									Atomic proportions									
	Pd	Pt	Ni	Fe	Te	Sb	Bi	As	Totals	Pd	Pt	Ni	Fe	Σ	Te	Sb	Bi	As	Σ
Merenskyite																			
1.	24.9	0.17	3.0	0.54	70.0	0.51	0.54	n.d.	99.66	0.82	<0.01	0.18	0.03	1.03	1.94	0.02	0.01	–	1.97
2.	27.5	0.17	1.8	0.59	68.0	0.65	1.0	n.d.	99.71	0.91	<0.01	0.11	0.04	1.06	1.89	0.03	0.02	–	1.94
Kotulskite																			
3.	43.6	0.21	1.8	0.56	38.4	15.8	1.2	n.d.	101.57	0.93	<0.01	0.07	0.02	1.02	0.68	0.29	0.01	–	0.98
4.	42.0	0.14	1.3	0.66	38.3	15.3	1.2	n.d.	98.90	0.92	<0.01	0.05	0.03	1.00	0.70	0.29	0.01	–	1.00
Keithconnite																			
5.	69.5	0.09	0.07	0.38	23.2	3.7	1.5	0.16	98.60	2.95	<0.01	<0.01	0.03	2.98	0.82	0.14	0.03	0.01	1.00
6.	70.0	0.74	n.d.	1.4	22.8	5.1	0.83	0.62	101.49	2.83	0.02	–	0.11	2.96	0.77	0.18	0.02	0.03	1.00
Mertieite II																			
7.	69.7	–	0.68	–	–	25.4	–	3.2	98.98	7.85	–	0.14	–	7.99	–	2.50	–	0.51	3.01

All the analyses were done on a JEOL-733 electron microprobe by WDS with exception of the mertieite II, done by EDS, at 20 kV, with a beam current of 12 nanoamperes, using the following X-ray lines and standards: PdL $\alpha$ , NiK $\alpha$ , SbL $\alpha$  (metals); AsK $\alpha$  (InAs). WDS analyses were done at 20 kV, with a beam current of 15 nanoamperes, using the following X-ray lines and standards: PdL $\alpha$ , PtL $\alpha$ , NiK $\alpha$ , FeK $\alpha$ , SbL $\alpha$  and BiL $\alpha$  (metals); TeL $\alpha$  (synthetic Pd<sub>0.9</sub>Ni<sub>0.1</sub>Te<sub>1.9</sub>) and AsK $\alpha$  (InAs). Some of the Fe and Ni reported may be partly due to secondary fluorescence from the host mineral(s), i.e., pentlandite, violarite or Fe-bearing silicate.

1. area 4, sample 85-7B,  $\pm$  5x11  $\mu$ m, attached to pentlandite in clinocllore(?) (Fig. 29, Table 3).
2. area 1, sample 85-7A,  $\pm$  8x10  $\mu$ m, attached to pentlandite/pyrite in serpentine(?) (Fig. 28, Table 3).
3. area 5, inclusion 1 sample 85-7B,  $\pm$  3x10  $\mu$ m, with merenskyite and violarite in clinocllore(?) (Fig. 30, Table 3).
4. area 5, inclusion 4 sample 85-7B,  $\pm$  7x7  $\mu$ m, with violarite in clinocllore(?) (Fig. 30).
5. area 30, sample 85-18,  $\pm$  4x10  $\mu$ m, in clinocllore(?).
6. area 5, sample 85-32-2B,  $\pm$  2x2.5  $\mu$ m, intergrown with laurite/hollingworthite in clinocllore(?) (Fig. 66, Table 3).
7. area 4, sample 85-32B,  $\pm$  6x12  $\mu$ m, in pyroxene(?) (Fig. 63, Table 3).

Table 7 – Electron microprobe analyses of sperrylite grains from Bird River sill samples

Analysis no.	Weight per cent										Atomic proportions										
	Pt	Pd	Rh	Ru	Os	Ir	As	Sb	S	Totals*	Pt	Pd	Rh	Ru	Os	Ir	Σ	As	Sb	S	Σ
1.	55.2	0.22	0.75	0.21	n.d.	0.11	42.6	0.39	0.48	100	0.96	0.01	0.02	0.01	–	<0.01	1.00	1.94	0.01	0.05	2.00
2.	56.9	n.d.	n.d.	n.d.	0.07	n.d.	42.7	0.30	0.05	100	1.01	–	–	–	<0.01	–	1.01	1.97	0.01	<0.01	1.98
3.	56.3	n.d.	0.31	n.d.	0.14	n.d.	43.1	n.d.	0.17	100	0.99	–	0.01	–	<0.01	–	1.00	1.98	–	0.02	2.00
4.	56.2	n.d.	0.30	n.d.	0.16	n.d.	43.2	n.d.	0.19	100	0.99	–	0.01	–	<0.01	–	1.00	1.98	–	0.02	2.00
5.	57.5	n.d.	0.10	n.d.	n.d.	n.d.	42.0	0.28	0.07	100	1.03	–	<0.01	–	–	–	1.03	1.95	0.01	0.01	1.97
6.	57.1	n.d.	n.d.	n.d.	n.d.	n.d.	42.9	n.d.	n.d.	100	1.01	–	–	–	–	–	1.01	1.99	–	–	1.99
7.	56.9	n.d.	0.18	n.d.	n.d.	0.12	42.6	n.d.	0.16	100	1.01	–	0.01	–	–	<0.01	1.02	1.97	–	0.02	1.99
8.	54.8	n.d.	1.9	0.49	n.d.	n.d.	41.9	n.d.	0.88	100	0.95	–	0.06	0.02	–	–	1.03	1.88	–	0.09	1.97
9.	55.6	n.d.	1.4	0.09	n.d.	0.11	42.0	0.35	0.44	100	0.97	–	0.05	<0.01	–	<0.01	1.02	1.92	0.01	0.05	1.98
10.	52.9	n.d.	1.7	n.d.	n.d.	1.3	41.1	2.4	0.62	100	0.92	–	0.06	–	–	0.02	1.00	1.87	0.07	0.06	2.00

\* Recalculated to 100%. The analyses were done by WDS on a JEOL-733 electron microprobe, operated at 20 kV, with a beam current of 25 nanoamperes, using the following X-ray lines and standards: PtL $\alpha$ , AsK $\alpha$  (synthetic PtAs $_2$ ); PdL $\alpha$ , RhL $\alpha$ , RuL $\alpha$ , OsL $\alpha$ , IrL $\alpha$ , SbL $\alpha$  (metals); SK $\alpha$  (pyrite). All the analyses were normalized to 100. Low totals may have been obtained by a combination of small size and geometry of the grains.

1. area 7, sample 85-32-2B,  $\approx$  8x9  $\mu$ m, in clinochlore(?) (Table 3).
2. area 6, same sample,  $\approx$  4x5  $\mu$ m, in clinochlore(?) (Table 3).
3. area 7, sample 85-07A,  $\approx$  8x18  $\mu$ m, in clinochlore(?) (Table 3) with minor pyrite attached (Fig. 32).
4. area 3, same sample,  $\approx$  10x13  $\mu$ m, in pyrite (Fig. 31) and surrounded by clinochlore(?) (Table 3).
5. area 13, sample 85-32A,  $\approx$  5x8  $\mu$ m, in serpentine(?) (Fig. 60, Table 3).
6. area 21, sample 85-18,  $\approx$  3x5  $\mu$ m, in clinochlore(?).
7. area 29, sample 85-18,  $\approx$  5x10  $\mu$ m, in clinochlore(?), close to chromite grain (Fig. 51).
8. area 28, sample 85-18,  $\approx$  10x15  $\mu$ m, in clinochlore(?), associated with keithconnite.
9. area 19, sample 85-18,  $\approx$  5x8  $\mu$ m, in clinochlore(?), associated with keithconnite (Fig. 52).
10. area 23, sample 85-18,  $\approx$  5x8  $\mu$ m, in clinochlore(?).

Table 8 - Electron microprobe analyses of hollingworthite and Os-Ir-Ru alloy from Bird River sill samples

85-32A-14			84-15-20		
	wt %	At. prop.		wt %	At. prop.
Rh	35.9	0.76	Os	45.8	0.41
Ru	3.8	0.08	Ir	38.7	0.34
Pt	5.6	0.06	Ru	13.8	0.23
Os	2.2	0.03	Rh	0.53	0.01
Ir	0.37	<0.01	Pd	0.20	<0.01
Ni	1.2	0.04	Pt	1.0	0.01
Fe	0.69	0.03			
As	33.3	0.97		100.0	
Sb	0.42	0.01			
S	14.9	1.02			
	98.38				

85-32A-14, hollingworthite ( $\approx 3 \times 5 \mu\text{m}$ ) occurring in serpentinite(?) and attached to pentlandite(?) (Fig. 65) sample 85-32A, area 14. Pd was not detected.

84-15-20, rutheniridosmine ( $\approx 2 \times 3 \mu\text{m}$ ) occurring in chromite (Fig. 21). Analysis normalized to 100% because of low total.

These analyses were done by WDS on a JEOL-733 electron microprobe, operated at 15 kV, with a beam current of 25 nanoamperes, using the following X-ray lines and standards: RuL $\alpha$ , RhL $\alpha$ , PdL $\alpha$ , PtL $\alpha$ , OsL $\alpha$ , IrL $\alpha$ , FeK $\alpha$ , NiK $\alpha$ , SbL $\alpha$  (metals); AsL $\alpha$  (InAs) and SK $\alpha$  (pyrite). Corrections were applied for the interferences between Ru, Rh and Pd, mentioned in Table 4.